CERN-TH.4556/86
DAMTP/86-19

DEEP INSIDE MATTER

M. Jacob
CERN -- Geneva

and

P.V. Landshoff
DAMTP, University of Cambridge

ABSTRACT

We review evidence that, at scales down to 10^{-18}m, matter shows a quark-gluon structure. At these distances, the unified picture provided by the standard model, which combines quantum chromodynamics with weak and electromagnetic interactions, gives a good description of experimental data. These successes suggest that new interesting phenomena are waiting to be discovered at scales of 10^{-19}m and provide encouraging hints for a better understanding of the structure of matter on the nucleon level, that is, at scales of 10^{-15}m.

CERN-TH.4556/86
DAMTP 86-19
September 1986

CONTENTS

1. INTRODUCTION

Preliminary survey of strong interaction physics

The numerous strongly-interacting particles discovered in the 1960's are now known to be composite systems, made of quarks. At the precision of present measurements, that is at the level of 10^{-18}m, quarks behave as pointlike objects. They carry a quantum number called colour, through which they couple to a vector field. The quanta of this field, the gluons, also carry colour. The coupling is determined from a gauge symmetry principle, with the unitary unimodular group SU(3) being the gauge group for colour. Quarks belong to the fundamental triplet representation of the gauge group, while gluons belong to the adjoint octet representation. The gauge theory, which has many similarities with quantum electrodynamics, is known as quantum chromodynamics or QCD. It was developed in the 1970's and is the theory of the strong interactions at the quark level.

A key property of quantum chromodynamics, which makes it very different from quantum electrodynamics, is asymptotic freedom. This means that the coupling of the theory becomes weak at short distance, so that at short distance the strong interaction is actually not so strong. The consequence is that a reaction in which a short-distance interaction occurs may be calculated in terms of a series expansion in powers of the coupling, that is by perturbation theory. At long distance, on the other hand, the strong interaction is very strong. Then perturbation theory cannot be used and calculation is very difficult.

One way to ensure that a short-distance interaction has taken place is to look for a reaction in which one or more particles is given a hard knock sideways, that is a reaction in which

there is large momentum transfer. In practice, in order to be able to apply perturbation theory, one needs a momentum transfer larger than about 10 GeV/c. From the uncertainty principle, we calculate that the associated distance is smaller than 10^{-17}m.

Such reactions are rather rare, but the great progress in particle physics during the last two decades has come about because we have learnt to concentrate attention on them. A large quantity of experimental data have now been accumulated, and the success with which it has been explained by QCD is impressive.

It is worth emphasising just how rare are these events. The physics at the CERN SPS proton-antiproton collider that has excited most interest corresponds to about one millionth part of the total cross-section.

The remaining events, which make up the bulk of the cross-section, cannot be described in terms of perturbation theory, because no short-distance interaction is involved and so there is no small coupling. Of the theoretical techniques being applied to the long-distance interaction, the most promising is to calculate in an approximation where continuous space-time is replaced by a lattice of discrete points. Lattice theory is being vigorously developed but has not yet reached a mature stage. Its first aim is to use QCD to obtain an understanding of the strongly-interacting particles (hadrons), that is how they are actually built out of quarks. For the present, though, the quark distribution in a hadron has to be parametrised empirically.

The increase of the coupling at large distance, and the direct colour coupling among gluons to which this is related, lead to some peculiar properties of the vacuum. According to present understanding, the vacuum behaves as a medium with

vanishingly small chromo-electric susceptibility: the colour field cannot freely penetrate it beyond a distance of about 1 fm from a colour source. So when two coloured quarks are pulled apart, the chromo-field between them does not spread through space in the same way as does the electric field between two charges; rather, it is confined to a tube of flux about 1 fm across. A simple application of Gauss's theorem shows that as the colour charges separate and the flux tube stretches, the energy stored in the field increases: there is about 1 GeV for each fm of flux-tube length.

This is what happens when a quark (or a gluon) is shot out sideways with large transverse momentum in a collision. As the flux tube stretches, the energy in it grows at the expense of the kinetic energy of the quark, until it far exceeds the mass energy of the lightest hadrons. It therefore readily materialises as hadrons (mostly pions), each carrying a fraction of the original momentum $\underline{p}$ of the quark. Each has a small component of momentum transverse to $\underline{p}$, which may be calculated by the uncertainty principle in terms of the width of the flux tube and is a few hundred MeV/c. So when p is large the hadrons associated with the stretching flux attached to the quark all emerge from the collision more or less in the same direction as $\underline{p}$. They are said to form a hadronic jet. So while one does not observe directly quarks (or gluons) shot aside during a collision, one finds in the resulting hadronic jet a clear kinematical signature of the underlying dynamics. Thus the jets are a powerful tool for the study of strong interactions of quarks and gluons.

Figure 1.1 shows one of the "Lego plots" which $p\bar{p}$ Collider experiments at CERN have made famous. What is displayed is the angular distribution of transverse energy

$$E_T = E \sin \theta$$

where θ is the angle with the line of the head-on-colliding beams. The angle ϕ is the azimuthal angle round this line. In a collision with centre-of-mass energy around 600 GeV, about 50 particles are produced. Most of them emerge with low transverse energy and are hardly visible on the Lego plot, whose vertical energy scale is chosen to match the tremendous amount of energy found in the two transverse jets. So the effect of interest, a quark or gluon large-momentum-transfer collision, shows up dramatically.

While the colour field is normally confined to flux tubes, this may not be so if the energy density, that is the temperature, is high enough. At small temperature T the flux tube between two points will tend to be stretched in a straight line between them, since longer tubes would carry more energy and so the Boltzmann factor e^{-E/k_BT} of statistical mechanics suppresses the probability of their occurring. This suppression reduces as T increases, until eventually the number of allowed configurations is such that the chromofield can effectively penetrate the whole vacuum. That is, at high T one expects that there is no longer confinement of colour, and there is nothing to prevent quarks moving fairly freely through long distances in the vacuum. This corresponds to a new state of matter, known as quark plasma.

Quark plasma presumably prevailed in the early Universe, while it was at high temperature in the first few microseconds

after the Big Bang. One hopes also to be able to create it in the laboratory, in high-energy heavy-ion collisions. This is the motivation for a major experimental program now beginning at CERN.

The clarity of the event structure in figure 1 provides a strong incentive to study hadronic collisions at still higher energy, so as to study the interaction at even shorter distance. So far, collisions with a centre-of-mass energy of a few hundred GeV have probed down to a distance of 10^{-18} m. There are plans in the United States and in Europe to increase the energy so as to reach down to 10^{-19} m or less. Attempts to unify the strong interaction with the electroweak, so as to form a single quantum field theory, raise important hierarchy problems. The danger is that our present picture of physics at the 100 GeV scale becomes blurred by radiative corrections associated with interactions having an energy scale some ten thousand billion times larger. Our tentative understanding calls for new effects at the TeV level in order to prevent this. Thus experiments that probe down to 10^{-19} m ought to discover some new physics. So the jet physics of today should be the prologue to further exciting discoveries within a decade.

Outline of article

In the next section we review how the concept of a pointlike structure within hadrons emerged from the study of deep inelastic lepton scattering. It soon became clear that these pointlike constituents are just the quarks that had earlier been used to explain the hadron spectrum. In this article we discuss quark dynamics and not quark statics, so we do not consider hadron spectroscopy - for a description of this, see Hendry and

Lichtenberg (1978).

The study of quark dynamics is the study of QCD. In §3 we review some of the many successful applications of perturbative QCD. We concentrate on hadronic collisions, particularly those in which there is large momentum transfer, with special emphasis on jet physics. Not covered in any detail are the very important and related results from electron-positron collisions and in particular the physics of quarkonia, bound states of a heavy quark and of its antiquark. Although they have contributed very greatly to our understanding, not only of jet physics but also of how quarks bind together to form hadrons, they have already been very widely reviewed. See, for example, the article by Wu (1984).

In §4 we turn towards a question which is often considered less glamorous, but which we consider to be very important. This is how to use our present knowledge to try to understand strong interactions at larger distance, for which perturbation theory is not applicable. These represent the overwhelming part of the total cross-section. Even though we do not yet have any fundamental understanding of these "soft" reactions, it has become clear in recent years that they have some surprisingly simple features. Some knowledge of these reactions is necessary for an understanding of the experiments which are attempting to produce quark plasma, which is the subject of §5.

Soft processes are associated with coherent effects among partons, whereas hard scattering involves the collision among two partons which behave incoherently with respect to the others. A transfer of a few GeV is needed to clearly select this incoherent behaviour. As the centre-of-mass energy increases, more and more

energetic partons become available for such incoherent behaviour. This induces a very interesting change in the nature of the typical process with in particular the emergence of mini-jets, which we discuss at the end of §4.

In the final section, we review expectations of what will be found in experiments an order of magnitude higher in energy than has so far been achieved. These will take us deeper inside matter, from the present 10^{-18} m down to 10^{-19} m.

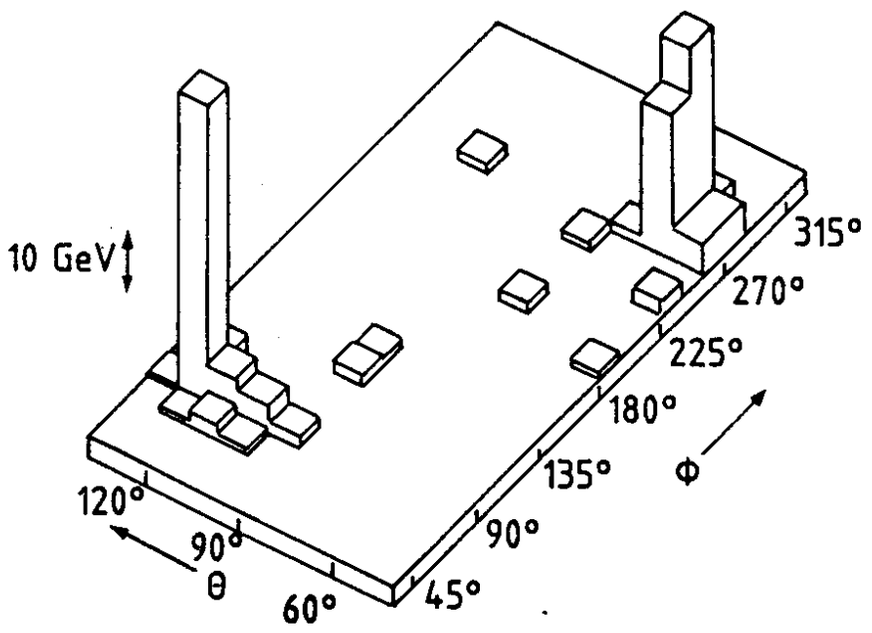

1.1 Evidence for jets at the $\bar{p}p$ Collider (UA2). The plot shows energy flow as a function of Θ and the azimuthal angle ϕ .

2. THE PARTON MODEL

Deep Inelastic Lepton Scattering

The experiments at SLAC in the late sixties on deep inelastic lepton scattering mark the beginning of high energy physics as we know it today. They led to the formulation of the parton model and hence to the idea that pointlike quarks are the fundamental hadronic objects to which currents couple, an idea that is central to the structure of modern gauge theories. We only briefly review deep inelastic lepton scattering and how it is analysed through the parton model. A more detailed account of the parton model has been given by Close (1979).

Consider then the set of reactions

$$\ell + N \to \ell' + X \tag{2.1}$$

where ℓ and ℓ' are leptons, N is a target nucleon, and X is a system of hadrons. These reactions are described by the diagram of figure 2.1, which shows the exchange of a virtual photon, W or Z between the lepton line and the target, so breaking up the target into a set of hadrons X. The main interest is in deep-inelastic events, where the momentum transfer q^2 of the photon , W or Z is large. As we shall see, these events probe the short-distance structure of the target nucleon.

An important feature of the quark parton model is that it relates a number of apparently rather different reactions:

$$\begin{aligned} &eN \to eX \\ &\mu N \to \mu X \qquad \text{(photon exchange)} \\ &\\ &\nu N \to \mu X \\ &eN \to \nu X \qquad \text{(W exchange)} \\ &\\ &\nu N \to \nu X \qquad \text{(Z exchange)} \end{aligned} \tag{2.2}$$

For definiteness, consider either of the two photon-exchange processes. For these, figure 2.1 corresponds to the reaction amplitude

$$e\,\bar{u}(\ell')\gamma_\lambda\,u(\ell)\qquad(g^{\lambda\mu}/q^2)\,A_\mu(\gamma^*N\to X)$$

$$=e\bar{u}(\ell')\gamma^\mu u(\ell)A_\mu/q^2 \tag{2.3}$$

Here u and $\bar{u}$ are spinor wave functions for the initial and final leptons, $g^{\lambda\mu}/q^2$ is the photon propagator, and A_μ is an unknown amplitude - it is determined by strong interactions and depends on the structure of the target nucleon.

In most experiments the final-state hadronic system X is not investigated, so to calculate the cross-section we must square the amplitude (2.3) and sum over X. Notice that in (2.3) μ is a dummy index of summation, so that when we multiply (2.3) by its complex conjugate we must introduce a second dummy summation index ν. The interesting part of the product is the factor

$$W_{\mu\nu}=\sum_X A_\mu A_\nu^* \tag{2.4}$$

$W_{\mu\nu}$ is a function of the target 4-momentum p, the photon 4-momentum q, and the spin vector of the target nucleon. In most experiments the target is unpolarised, so that we must average over its spin states, leaving $W_{\mu\nu}$ a function of p and q only. Because it is a tensor, its structure must therefore be

$$W_{\mu\nu}=-g_{\mu\nu}W_1+p_\mu p_\nu W_2+\tfrac{1}{2}i\epsilon_{\mu\nu\alpha\beta}q^\alpha p^\beta W_3+\ldots\ldots \tag{2.5}$$

where W_1 , $W_{2,...}$ are functions of the Lorentz scalars q^2 and $\nu = p.q$. [Notice that it is usual to name the coefficient of $g_{\mu\nu}$ as W_1, but some authors write W_2/M^2 instead of W_2, and often $\nu = p.q/M$, where M is the target mass.] In the case of photon exchange, parity conservation requires $W_3 = 0$ but W_3 is needed for the W and Z exchange reactions. The terms not written in (2.5) involve

$$q_\mu p_\nu, \qquad p_\mu q_\nu, \qquad q_\mu q_\nu \tag{2.6}$$

However, remember that $W_{\mu\nu}$ must be multiplied by a factor coming from the lepton line, and

$$\bar{u}(\ell')\gamma.q\,u(\ell) = \bar{u}(\ell')\gamma.(k-k')\,u(\ell) \tag{2.7}$$

where k and k' are the momenta of the initial and final leptons ℓ and ℓ'. So the Dirac equation implies that the terms (2.6) give contributions that either vanish, or are proportional to lepton mass and so negligibly small. We therefore limit ourselves to the three terms explicitly written in (2.5).

The variable q^2 is a momentum transfer and so it is negative. One commonly defines the two new variables

$$Q^2 = -q^2$$

$$\omega = 2\nu/Q^2 \tag{2.8}$$

The dimensionless variable ω is called the Bjorken scaling variable. In the way we have defined them, W_1 and νW_2 are dimensionless functions. It is usual to write

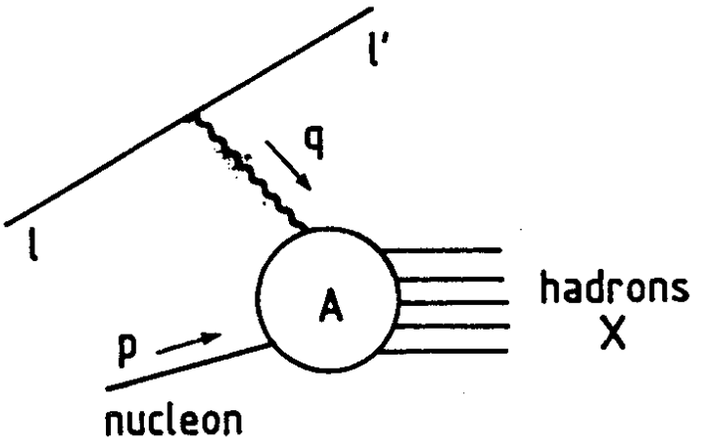

2.1 Deep inelastic lepton scattering through the exchange of a virtual photon, W or Z.

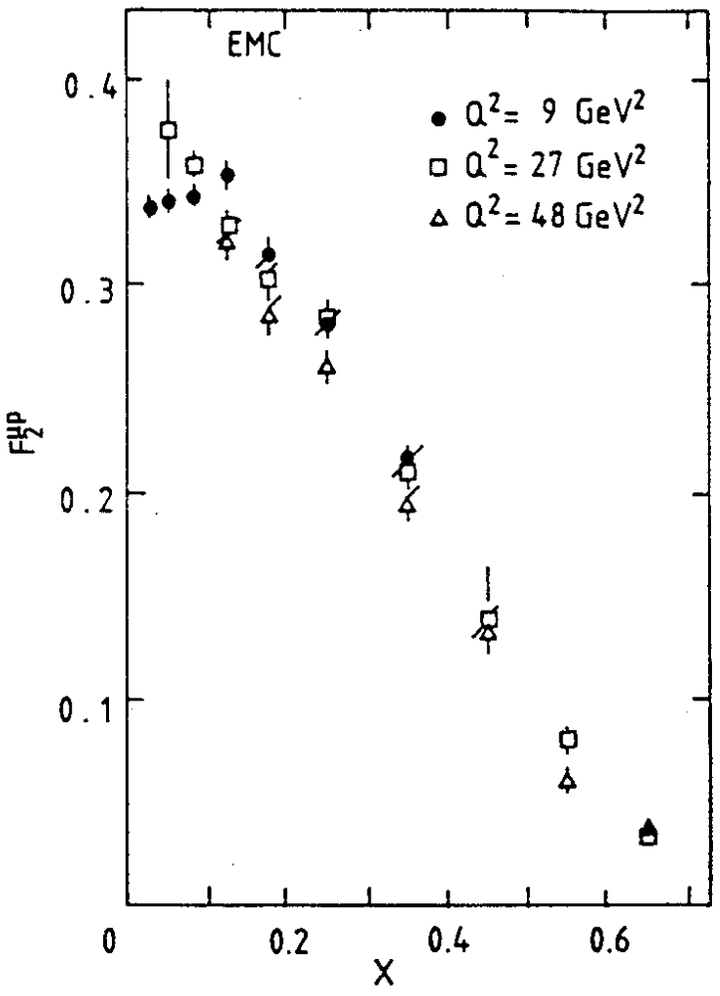

2.2 In deep inelastic muon scattering the structure function F_2 at each value of $x = 1/\omega$ is almost independent of Q^2 .

$$W_1(q^2,\nu) = F_1(\omega,Q^2)$$

$$\nu W_2(q^2,\nu) = F_2(\omega,Q^2) \qquad (2.9)$$

Experiment finds that when Q^2 is large, to a very good approximation F_1 and F_2 depend only on ω and not on Q^2. In the case of the neutrino processes, the same applies to $F_3(\omega,Q^2) = \nu W_3$. This property is known as Bjorken scaling. See the data in figure 2.2.

This important discovery implies that whatever structure in the nucleon is responsible for absorbing the virtual photon, it is effectively pointlike. For suppose that F_1 and F_2 did vary with Q^2. Then, because they are dimensionless, they must be functions of Q^2/Q_0^2 for some fixed Q_0. Then the cross-section would depend on a fixed length $1/Q_0$.

So Bjorken scaling suggests that the virtual photon couples to pointlike objects in the nucleon. These objects are called partons, and a natural guess is that the partons are quarks since they couple to the Weak and Electromagnetic currents. This assumption is reinforced by another experimental finding, that to a good approximation

$$F_1(\omega) = \tfrac{1}{2}\omega F_2(\omega) \qquad (2.10)$$

This is known as the Callan-Gross relation. It may be shown to imply that the virtual photon is transversely polarised and, more important, that the partons have spin ½. Spin 0 partons would give $F_1(\omega) = 0$.

The picture we have, then, is that the virtual photon is absorbed by a quark parton (figure 2.3). However, this raises a big problem: no quarks have been observed in the final state. The solution to this confinement problem is not yet well understood, but it must be that somehow a final-state interaction prevents fractionally-charged objects from escaping into the final state. Experiment finds that, instead of a quark, there is a jet of hadrons as already said in section 1. A jet is a group of particles whose momenta are approximately parallel and although we do not fully understand how this comes about, the idea is that it is associated with the chromo-electric field, which is the QCD analogue of the electric field. As the quark tries to escape from the vicinity of its parent nucleon, a chromo-electric field is set up between it and the remaining nucleon fragments. We have seen that, if for some reason this field is confined to a tube instead of spreading out in all directions, its energy increases as the quark gets further away, this energy being provided by the slowing down of the quark. Coming back with slightly different words to the hadronization process one may say that when the field energy is high enough, it can create new quark-antiquark pairs. The antiquark fuses with the original quark to form a meson, and the new quark tries to escape. The process is then repeated, so that further mesons are created and form a jet. Thus figure 2.3 becomes figure 2.4a. The particle momenta in the photon, W, Z - nucleon centre-of-mass frame are drawn in figure 2.4b, which shows also the jet associated with the residual nucleon fragments.

The key assumption in the calculation of the structure functions F_1, F_2, and F_3 in the parton model is that, in a frame where the nucleon 3-momentum $|\tilde{p}|$ is large, the 4-momentum of the

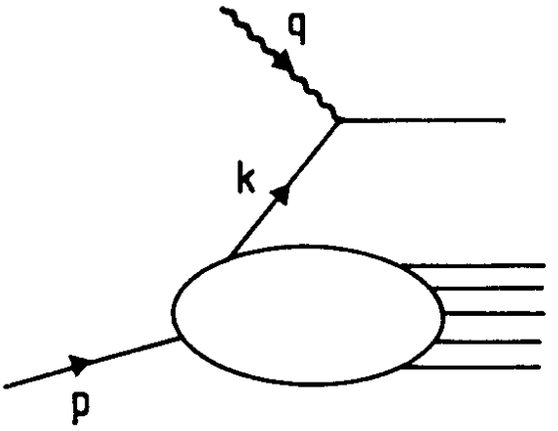

2.3 Absorption of the virtual photon by a quark parton.

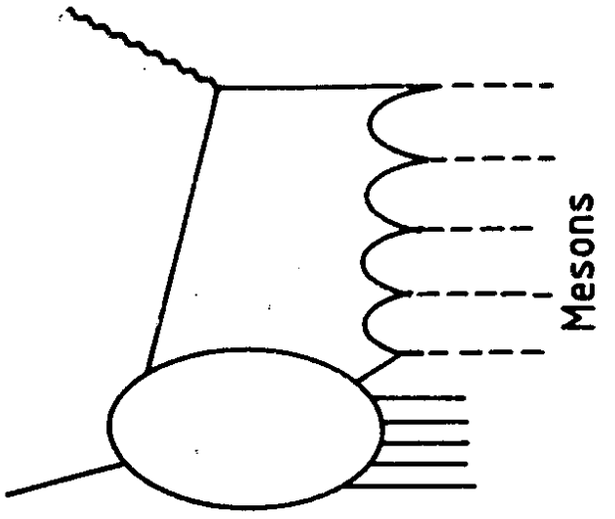

a)

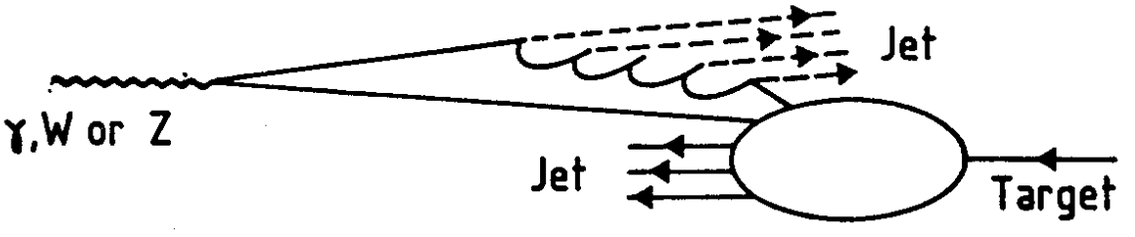

b)

2.4 Jet creation : (a) the effect on figure 2.3 of final-state interaction; (b) particle momenta in the photon N centre-of-mass frame, for the virtual quantum-nucleon interaction.

constituent partons is almost parallel to p:

$$k \approx xp \tag{2.11}$$

This amounts to saying that in the nucleon rest frame the partons do not have large momentum. One introduces an x distribution for each parton flavour:

$q(x)dx$ = the expectation value of the number of partons of flavour q with x in the range $(x, x+dx)$ $(q = u,d,s,c,b...)$ (2.12)

One also uses the charge symmetry of the strong interactions, so that for example the u-distribution in the proton is the same as the d-distribution in the neutron. Finally, one uses the couplings of the photon, W and Z to leptons and quarks that are given by the Salam-Weinberg model. For the details of the calculation, see the article by Close (1979).

An important result that derives from the kinematics of the parton model is that

$$x = 1/\omega \tag{2.13}$$

According to (2.8), ω is measured from the momenta of the initial and final leptons, so this result says that by seeing how the lepton is scattered we deduce the fractional momentum x of the quark that is responsible for the scattering. The various reactions (2.2) are all calculable in terms of the quark distributions q(x), for example

$$F_2^{\mu P}(\omega,Q^2) = \frac{4}{9}\left[xu(x) + x\bar{u}(x)\right] + \frac{1}{9}\left[xd + x\bar{d} + xs + x\bar{s}\right] \qquad (2.14)$$

with contributions from the heavier quarks switching on at larger values of Q^2.

It is of course not trivial that the various reactions μp, μn, νp, $\bar{\nu} p$, νn, $\bar{\nu} n$ can all be calculated in terms of the same functions u(x), d(x),... It however works very well when we use the known couplings of the quarks to the Electromagnetic and Weak fields. That this works well is an important test of the quark parton model.

By combining data from the various reactions, one may extract the separate parton densities u(x),d(x).... The resulting picture of the nucleon is a little more complicated than the original three-quark structure postulated by Gell-Mann and Zweig. Instead

$$\text{proton} = (uud) + \begin{matrix}\text{neutral sea of} \\ q\bar{q} \text{ pairs and} \\ \text{gluons}\end{matrix} \qquad (2.15)$$

The (uud) are called <u>valence quarks</u> and give the proton its quantum numbers, while the sea is neutral and is the same for proton and neutron. It seems to be valid to regard each parton distribution as a sum of valence and non-valence parts, though strictly one might expect some quantum- mechanical interference between the two. Thus

$$\begin{aligned} x\,u(x) &= V(x) + N(x) \\ x\,\bar{u}(x) &= \qquad N(x) \end{aligned} \qquad (2.16)$$

where N(x) is the non-valence part. Experiment seems to find that the sea is SU(2) invariant, so that the d-quarks have the same non-valence distribution. The simplest assumption is that their valence distribution is again proportional to V(x), but with a factor ½ because there are half as many valence d quarks in the proton as valence u quarks:

$$x\,d(x) = \tfrac{1}{2}V(x) + N(x)$$

$$x\,\bar{d}(x) = N(x) \qquad (2.17)$$

This assumption works well enough as a first approximation, though it is not exact because it is now well established that actually the d-quark distribution falls off more rapidly than the u-quark distribution as $x \to 1$. The distributions of the heavier quarks are entirely non-valence. Their shapes seem to be the same as that of N(x), but their normalisations are probably rather smaller, even when Q^2 is large enough for them to be fully "switched on". The experimental results are described by Eisele (1986) and Scott (1986).

In figure (2.5) we sketch the valence and non-valence distributions. Notice that N(x) is very small except at small values of x. The behaviour of the two functions as $x \to 0$ is controlled by Regge theory, which we describe briefly in §4. This makes N(x) go approximately to a constant at very small x, corresponding to pomeron exchange, while

$$V(x) \approx x^{1-\alpha(0)} \qquad (2.18)$$

Here $\alpha(0)$ is the intercept of the exchange-degenerate (ρ,ω,f,A_2)

trajectory, with $\alpha(0) \approx \frac{1}{2}$ (to which we come back in section 4). So for very small x,

$$q(x) \approx \frac{1}{x} N(x) \tag{2.19}$$

for $q = u,d,\bar{u},\bar{d}....$ Hence the number of partons of each flavour with fractional momentum less than ϵ,

$$\int_0^{\epsilon} dx\ q(x) \tag{2.20}$$

diverges logarithmically. That is the sea contains a very large number of very-small-x partons.

Finally, one may calculate the total fractional momentum carried by all the quarks and antiquarks:

$$\int_0^1 dx\ x[u(x) + \bar{u}(x) + d(x) + \ldots] \tag{2.21}$$

Experiment finds a value near to $\frac{1}{2}$. The other half of the momentum of the target must be carried by objects to which the photon, W and Z do not couple. We have no reason to doubt that these are just the gluons of QCD.

The peculiar properties of deep inelastic scattering were first obtained by Bjorken (1969) in the framework of a field theoretic approach. The quark parton model due to Feynman then offered a simple and powerful physical picture. Its deep validity was then justified by its successful extension to other processes.

The Drell-Yan Process and W production

It is indeed obviously necessary to test the parton model by applying it to other reactions. For this purpose, an important reaction is the Drell-Yan process

$$pp \rightarrow \mu^+\mu^- + X \qquad (2.22)$$

where, as usual, X is an undetected system of hadrons. For large values of the invariant mass $m_{\mu\mu}$ of the muon pair (and such that the pair is not formed from the production and decay of a resonance), the reaction is described by the Drell-Yan quark-antiquark fusion mechanism of figure 2.6. We have not shown in this figure possible additional final-state interactions between the two jets of hadrons. Certainly these are needed to achieve confinement, as we discussed for the case of deep inelastic scattering. However, DeTar, Ellis and Landshoff (1975) have shown that they do not change the value of the inclusive cross-section for the case when only the final-state muons, and not the hadrons, are detected.

It will be seen that the amplitudes at the top and bottom of figure 2 are the same as the amplitude that occurs in the deep inelastic scattering diagram of figure 2.3. So the Drell-Yan process may be calculated in terms of the same parton distributions u(x), d(x) ... that occur in deep inelastic scattering. This close connection between two very different sorts of reaction is all the more remarkable in that the Drell-Yan process involves a timelike photon, with $q^2 = m_{\mu\mu}^2 > 0$, while in deep inelastic scattering $q^2 < 0$.

According to equation (2.11), in a frame where a hadron is

moving fast its constituent partons move almost parallel to it. So we have asymptotically when the parton transverse momentum can be neglected,

$$k_1 \approx x_1 p_1, \quad k_2 \approx x_2 p_2 \tag{2.23}$$

So $q^2 = (k_1 + k_2)^2 = (x_1 p_1 + x_2 p_2)^2 \approx 2 x_1 x_2 p_1 \cdot p_2$, or

$$x_1 x_2 \approx \tau \tag{2.24}$$

where $\tau = q^2/s$, with $s = (p_1 + p_2)^2 \approx 2 p_1 \cdot p_2$. In the centre-of-mass frame

$$p_1 \approx (\tfrac{1}{2}\sqrt{s}, 0, 0, \tfrac{1}{2}\sqrt{s}), \quad p_2 \approx (\tfrac{1}{2}\sqrt{s}, 0, 0, -\tfrac{1}{2}\sqrt{s}), \tag{2.25}$$

and so the longitudinal component of q is $q_L = (x_1 p_1 + x_2 p_2)_z = \tfrac{1}{2}\sqrt{s}(x_1 - x_2)$. Thus

$$x_1 - x_2 = x_F \tag{2.26}$$

where x_F is the Feynman scaling variable, $x_F = q_L/\tfrac{1}{2}\sqrt{s}$. Thus x_1 and x_2 may be found by measuring x_F and τ, and then solving the simultaneous equations (2.24) and (2.26). So, as in deep inelastic scattering, the parton fractional momentum x may be found by measuring the lepton momenta.

Calculation gives

$$\frac{d^2\sigma}{dx_F d\tau} = \frac{1}{3} \frac{4\pi\alpha^2}{3m_{\mu\mu}^2} \frac{1}{x_1 + x_2} F(x_1, x_2) \tag{2.27}$$

with

$$F(x_1,x_2) = \frac{4}{9}u(x_1)\bar{u}(x_2) + \frac{1}{9}d(x_1)\bar{d}(x_2) + (x_1 \longleftrightarrow x_2) + \ldots \quad (2.28)$$

where we have not written contributions from heavier quarks. The factor $\frac{1}{3}$ in (2.27) is present because of colour: the quark and antiquark can only fuse to form a photon if their colours are equal and opposite, and there is a 1 in 3 chance of this being true. For details of the calculation, see Kenyon (1982).

Taking the parton distributions from deep inelastic scattering, one can calculate (2.27) completely. The agreement with experiment is extremely good for the variation of the cross section with energy, $m_{\mu\mu}$ and x_F, but to get its magnitude right one has to multiply by the factor

$$K \approx 2.2 \quad (2.29)$$

This K-factor is believed to originate in QCD corrections to the Drell-Yan mechanism. We shall explain this further in §3.

The Drell-Yan process is important for a number of reasons. Not only is it a non-trivial test of the parton model, it also enables one to measure structure functions for hadrons other than nucleons. For example, the structure function F_2 of the pion cannot be measured in deep inelastic scattering because pion targets are not possible, but measuring the Drell-Yan process with a pion beam gives the same information. The result is that the structure function of the pion is found to fall off rather more slowly as $x \to 1$ than does that of the nucleon.

Another, very important, feature of the Drell-Yan mechanism is that it allows W and Z production in hadronic collisions - in figure 2.6 the virtual photon is replaced by the W or Z. The

cross-sections for the CERN $\bar{p}p$ collider are at the nanobarn level. The discovery of the particles exactly as predicted is a triumph not only for the Drell-Yan model but also, more importantly, for the Salam-Weinberg electroweak theory. The story is told by Watkins (1986).

e^+e^- Annihilation

To lowest order in the electromagnetic coupling α, the process

$$e^+e^- \rightarrow \mu^+\mu^- \tag{2.30}$$

is calculated from the single diagram of figure 2.7. The result is

$$\frac{d\sigma}{d(\cos\theta)} = \frac{\pi\alpha^2}{2s}(1+\cos^2\theta) \tag{2.31}$$

where $\sqrt{s}$ is the centre-of-mass energy and θ the angle at which the μ^+ emerges relative to the e^+. If one replaces the muon line in figure 8 by a quark line, one obtains a possible mechanism for the process

$$e^+e^- \rightarrow \text{hadrons} \tag{2.32}$$

The only difference in the calculation of the new diagram is that the quark has fractional charge e_i instead of integral charge e, so one has

$$R = \frac{\sigma(e^+e^- \rightarrow \text{hadrons})}{\sigma(e^+e^- \rightarrow \mu^+\mu^-)} = 3 \sum_{i=u,d,\ldots} (e_i/e)^2 \tag{2.33}$$

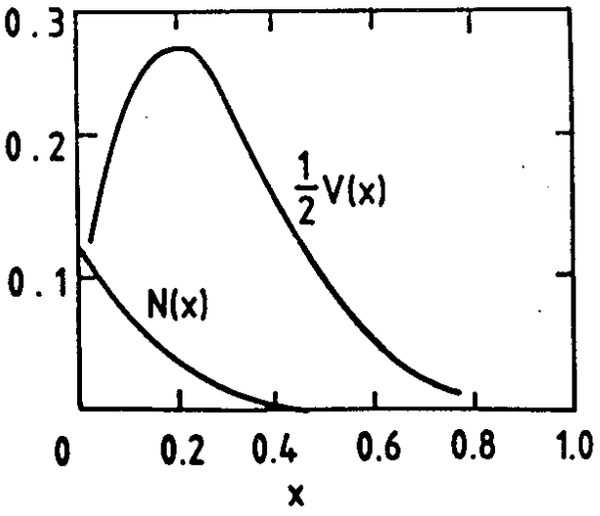

2.5 Sketches of the distributions of valence and non-valence quarks in the nucleon.

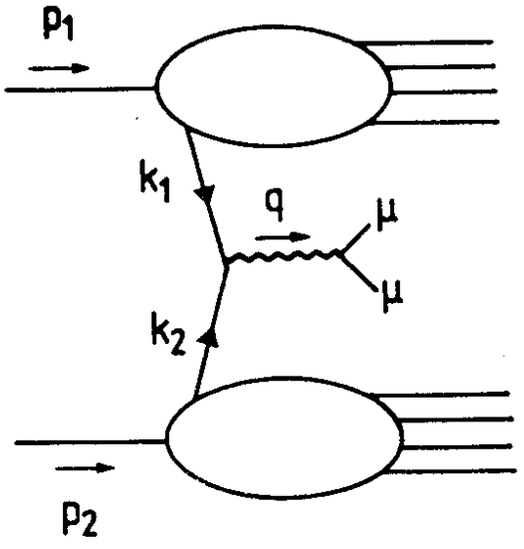

2.6 The Drell-Yan mechanism.

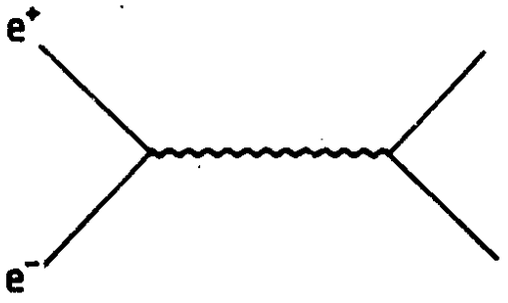

2.7 Diagram for $e^+e^- \rightarrow \mu^+\mu^-$ or $q\bar{q}$.

The factor 3 here enters because each flavour i of the quark can be produced in 3 versions of different colours. Data for R are shown in figure 2.8; for $\sqrt{s}$ between 12 and 45 GeV they fit very well to the expression (2.33), with i = u,d,s,c,b included. It is evident that there is no room in the data for the inclusion of a t quark, which would increase R by 12/9. Notice that these data are the best evidence for the need for three colours.

As in deep inelastic scattering, the q and $\bar{q}$ are not seen in the final state: instead, one sees a pair of jets. Because the experiments are performed with the e^+ and e^- colliding head-on, the two jets emerge back-to-back. A typical event is seen in figure 2.9.

Evidence that the two jets are indeed associated with quarks comes from the angular distribution of the jet axis (the direction of the total momentum of the particles in a jet) relative to the beam direction. As the quarks have spin ½ this angular distribution should be $1+\cos^2\theta$ as in (2.31), and this is what is found. See Wu (1984). Spin 0 partons would instead give $\sin^2\theta$, which does not agree with experiment.

One may investigate whether the jets have the same structure as the forward jet in deep inelastic scattering (see figure 2.4). One distribution that is important is the jet fragmentation function. The jet axis is identified and the component p_L of the momentum of each hadron along the jet axis is measured. Define

$$z = p_L/E^{Jet} \qquad (2.34)$$

where E^{Jet} is the total energy of the jet. It is then found that, for each type of hadron, the distribution dN/dz satisfies

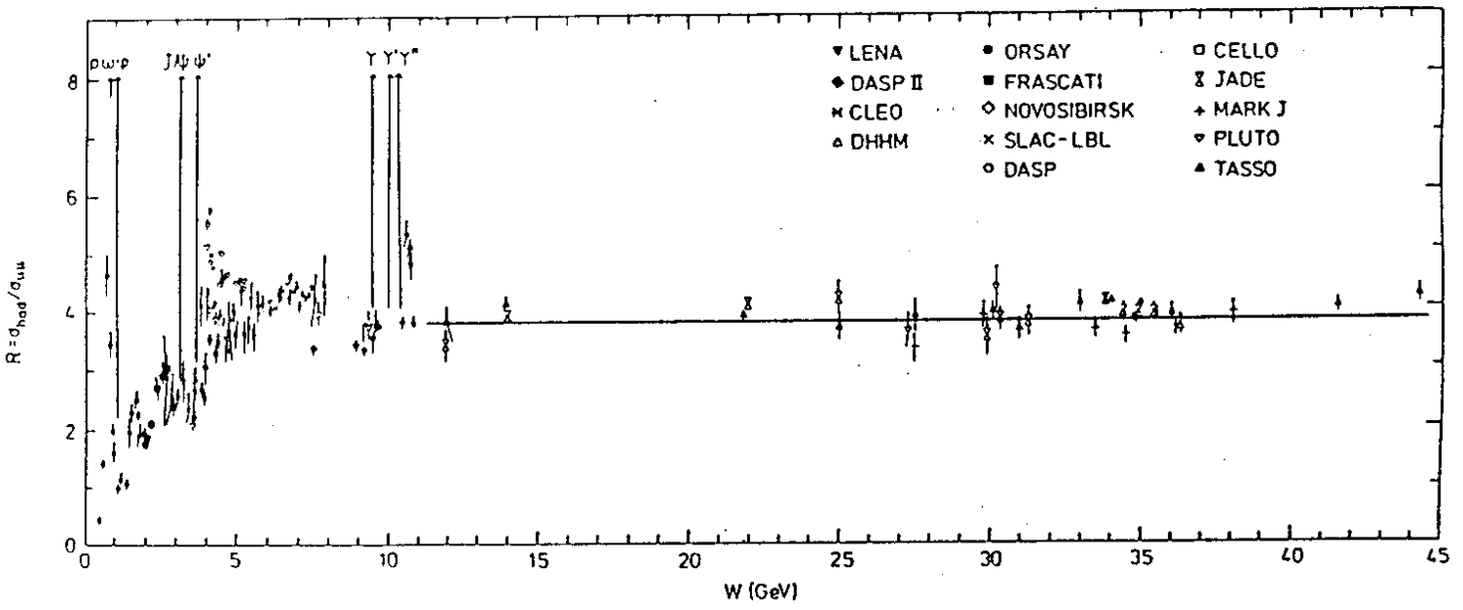

2.8 Data for $R_{e^+e^-}$. The horizontal straight line shows $\Sigma(e_i/e)^2$ for u,d,s,c,b.

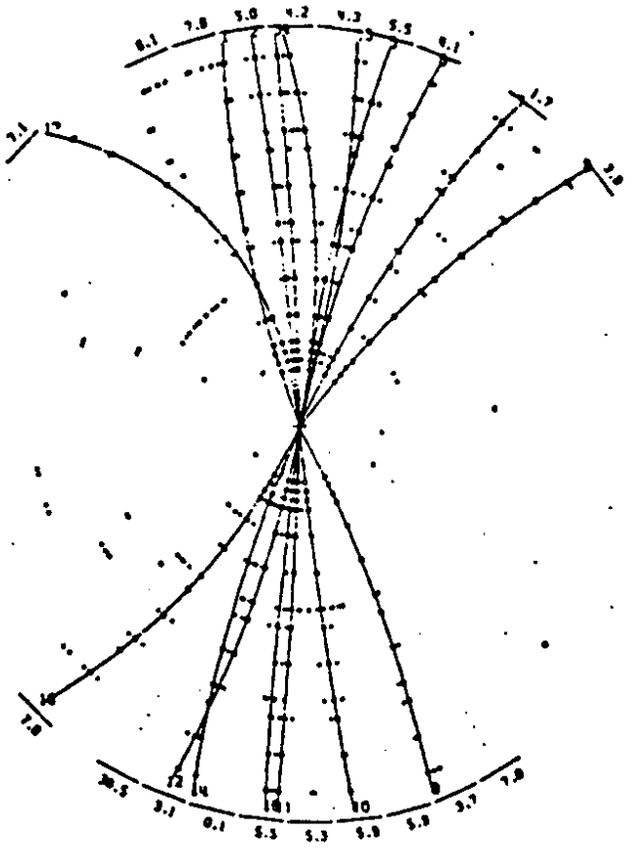

2.9 A typical two-jet event in e^+e^- annihilation (TASSO).

an approximate scaling law: to a first approximation it is a function of z only, independent of p^{Jet}. (See figure 2.10). This scaling is theoretically related to Bjorken scaling in deep inelastic scattering. Just as in deep inelastic scattering, nowadays the interest is not so much in how well it is satisfied, but more in how much it is violated. Very similar jet fragmentation functions are measured in deep inelastic scattering, in experiments that look at the final-state hadrons.

We have thus seen how the concept of partons provides unity to three a priori very different processes: deep inelastic lepton scattering, lepton pair production in hadronic interactions and electron-positron annihilation into hadrons. The analysis of these processes leads one to identify partons with quarks. One could also predict correctly the production cross section of the W and Z bosons at the CERN $p\bar{p}$ Collider. While these progresses were first of a phenomenological nature, power and accuracy was quickly gained considering them in the framework of an actual theory, QCD. This is what we now turn to.

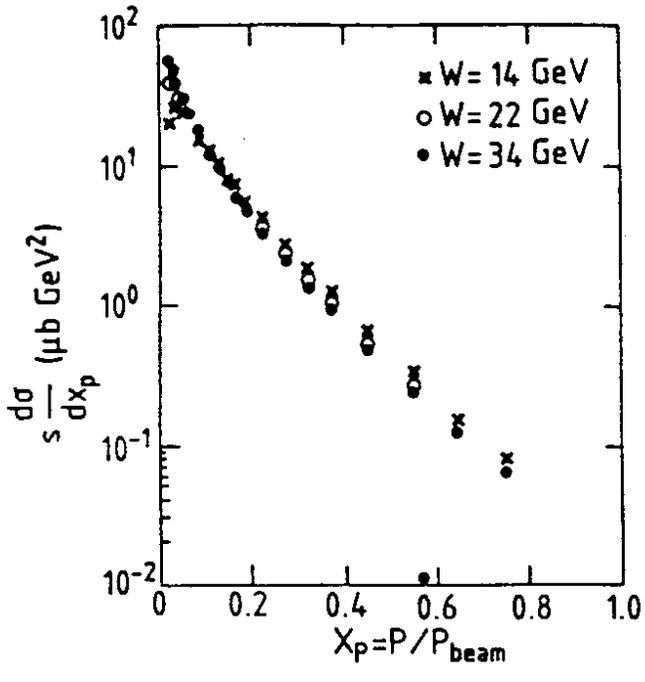

2.10 Longitudinal momentum distribution of charged particles produced in e^+e^- annihilation (TASSO).

3. PERTURBATIVE QCD

We have seen that the simple parton model gives a good explanation of a number of effects. We now consider how it has to be corrected by including gluon radiation corrections. The parton model is now to be regarded as the zeroth-order term in a QCD perturbation theory expansion.

Perturbative QCD has a very large number of successes, some of which are reviewed in this section. Taken together, the evidence for the correctness of QCD is very impressive. It should be recognised, however, that there are limitations to the accuracy of all the calculations. These arise from two main sources, both of which we shall briefly describe. First we cannot calculate the so-called higher twist contributions, which are nonleading power corrections to the perturbative QCD calculations. Secondly one finds that there is substantial renormalisation-scheme dependence in the calculations, and we have no certain way of choosing the best scheme for a given calculation. This affects calculations beyond leading order. Rather than starting from the QCD Lagrangian and work out predictions, we shall consider some specific processes and show how QCD improves on the parton model of section 2.

Jet Widening in e^+e^- Annihilation

We have explained that the simple parton model predicts that in high-energy e^+e^- annihilation into hadrons the final state should consist of two jets. Suppose that this is assumed to be true, and that the jet axis has been found. One way to do this is to guess a direction for the axis, measure the transverse momentum p_T of each particle relative to this direction, and then vary the direction so as to minimise Σp_T^2. Figure 3.1 shows the

p_T distribution relative to the resulting jet axis, which is seen to become wider as the centre-of-mass energy increases.

This jet widening is understood in terms of gluon radiation: one of the quarks in figure 2.7 radiates a gluon, as is shown in figure 3.2. In most events of this type, the gluon emerges almost in the same direction as that of the quark with which it is associated, so resulting in a two-jet event with one jet slightly widened. Sometimes, however, the gluon comes out in a different direction from the quark. This is far more spectacular with a clear 3 jet structure. This is the way evidence for the gluon could be claimed at PETRA in 1979. Gluons, like quarks, are subject to a confinement law and are not detected as such; what is seen in these events are three jets of ordinary hadrons. An example is shown in figure 3.3.

Jet Fragmentation

There are a number of models for calculating how a quark (or gluon) jet fragments into hadrons. A useful comparison of the models was made by Saxon (1985).

The original model of quark fragmentation, proposed by Niedermayer (1974) and by Feynman and Field (1978) is crude but effective. It assumes that a quark fragments independently of whatever else emerges from the reaction. The model has as input a primary fragmentation function: this describes the z distribution of the primary meson, produced by the fusion of the original quark with the antiquark member $\bar{q}$ of a $q\bar{q}$ pair created out of the vacuum (see figure 3.4). The relative probabilities of creating the different possible flavours of quark from the vacuum are chosen such that the output of the calculation fits experiment. It is found that the heavier the flavour, the less probable must

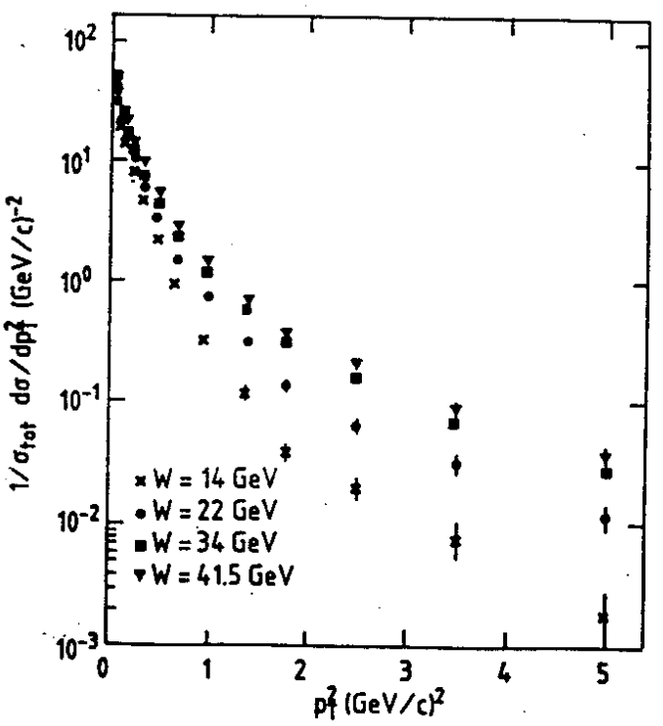

3.1 P_T distribution relative to the jet axis in e^+e^- annihilation (TASSO).

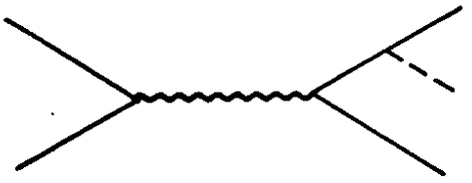

3.2 Gluon radiation from a quark (or antiquark) in e^+e^- annihilation.

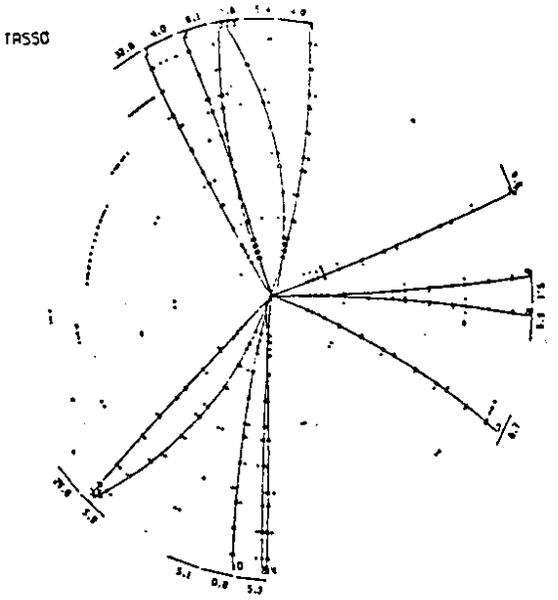

3.3 A three-jet event in e^+e^- annihilation.

be its creation. The quark q that emerges from the primary fusion then undergoes a similar fate to the original quark. This process is repeated until the residual quark has small momentum; what happens then is left somewhat uncertain in the model.

Today's models improve on this in various ways. By abandoning the independent-fragmentation hypothesis they are able to describe the slow hadrons properly. They also describe the kinematics correctly: the independent-fragmentation model supposes that at each stage the quark that emerges from the fusion is "on shell", but actually this cannot be so. Also, and very important, while the fusion process that produces a meson must be nonperturbative, nowadays it is realised that one must take into account the perturbative radiation of gluons in the initial stages of the reaction, before the fusions that finally produce the mesons take place.

Although today's models looked rather different from one another when they were first proposed, they have become more similar over the years. Figure 3.5 depicts the Webber model; it shows the perturbative radiation of gluons, followed eventually by the production of pairs of resonances by (non-perturbative) quark fusion. It is generally agreed that in fact most of the pions seen in the final state are actually the decay products of resonances.

The current versions of the models all agree rather well with data and with each other. An example is shown is figure 3.6, where four models are compared with data for the variation with angle of the energy flow in three jet events in e^+e^- annihilation. The models describe not only quark jets but also gluon jets. They agree, with support from data, that gluon jets are

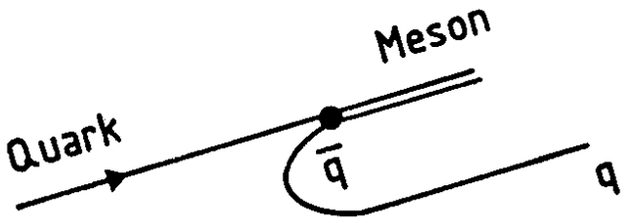

3.4 Formation of the primary meson in a quark jet.

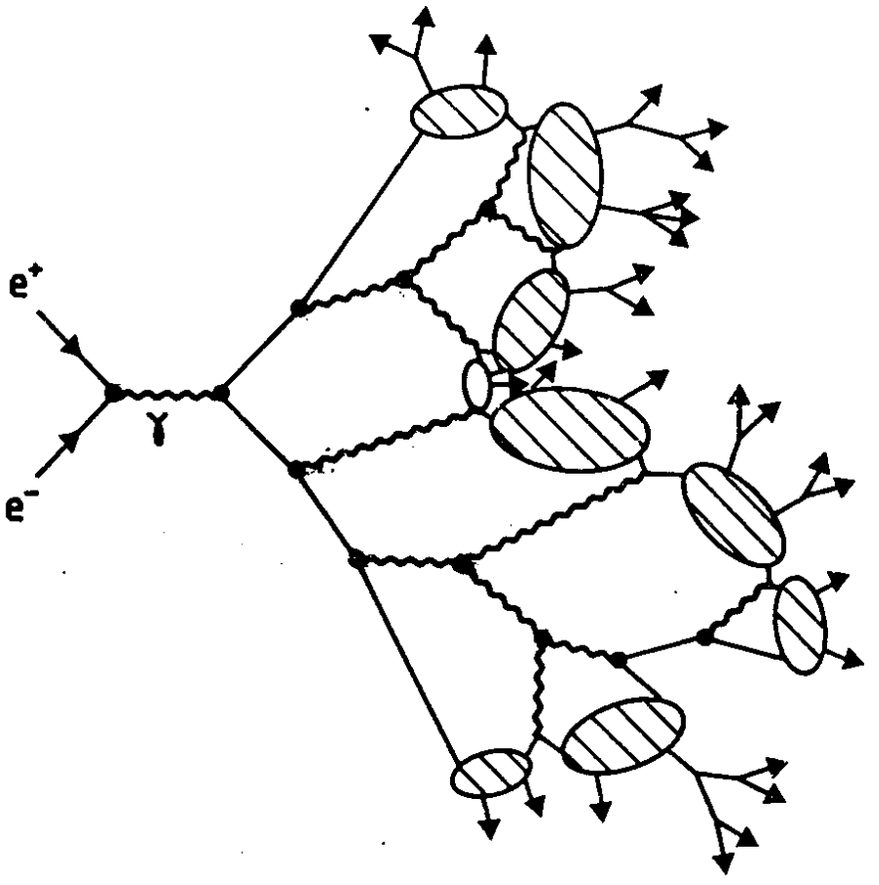

3.5 The Webber model (perturbative evolution followed by phenomenological hadronization).

softer, that is they yield fewer fast hadrons and more slow ones. One reason for this is that gluons carry more colour than quarks, and therefore they radiate gluons more copiously before the hadronisation.

While one may stress global agreement, one may also focus on differences. The dip close to 90° in figure 3.6, correctly predicted by the Webber model, corresponds to a destructive interference among soft gluons radiated by quarks. This is regarded as the correct QCD interpretation. The Lund model gets it phenomenologically describing the gluon as a pinch on the colour string between the two quarks. The other two models, describing the three jets independently, miss it.

Note that the primary meson in a quark jet is very likely to be the fastest meson. One consequence of this is that, for example, a u quark is more likely to have a fast π^+ than a fast π^- among its fragmentation products. So if in e^+e^- annihilation there is a fast π^+ in one direction, the fastest meson in the opposite direction is more likely to be a π^- than a π^+. Another consequence is that charmed hadrons are usually found with larger momentum than most of the pions. To understand this, remember that $c\bar{c}$ pair creation out of the vacuum is rather rare, so the the D meson is most probably the primary meson in the fragmentation of a c quark. Being heavy the D meson also takes a relatively large fraction of the momentum of any hadronic system it may belong to. Data are shown in figure 3.7.

Scale-Breaking in Deep Inelastic Lepton Scattering

In the presence of QCD corrections, the simple parton model of figure 2 is regarded as the zeroth-order term in a perturbation expansion in powers of the QCD coupling α_s. While the top

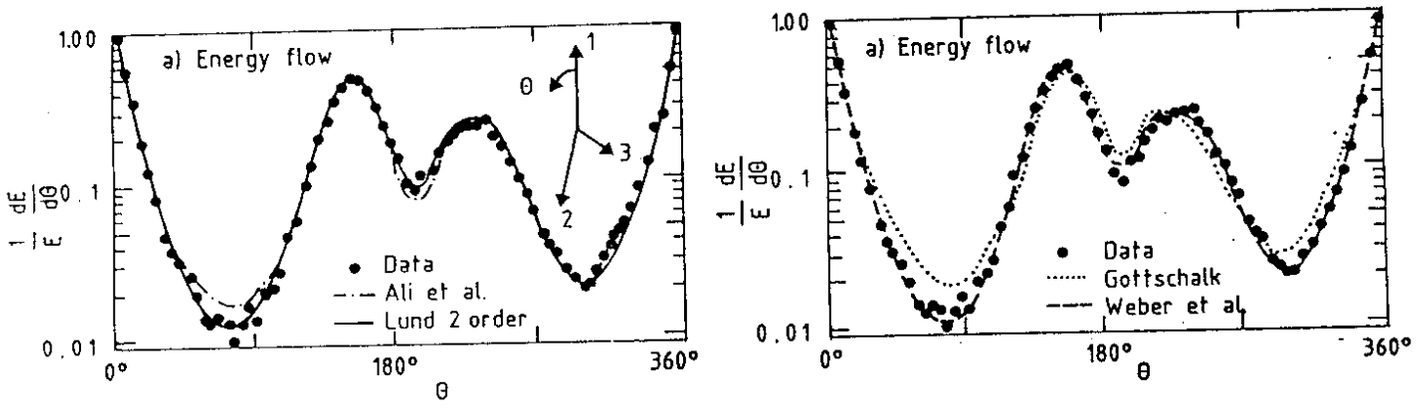

3.6 JADE data for the angular distribution of the energy flow in 3-jet events in an e^+e^- annihilation, compared with model calculations.

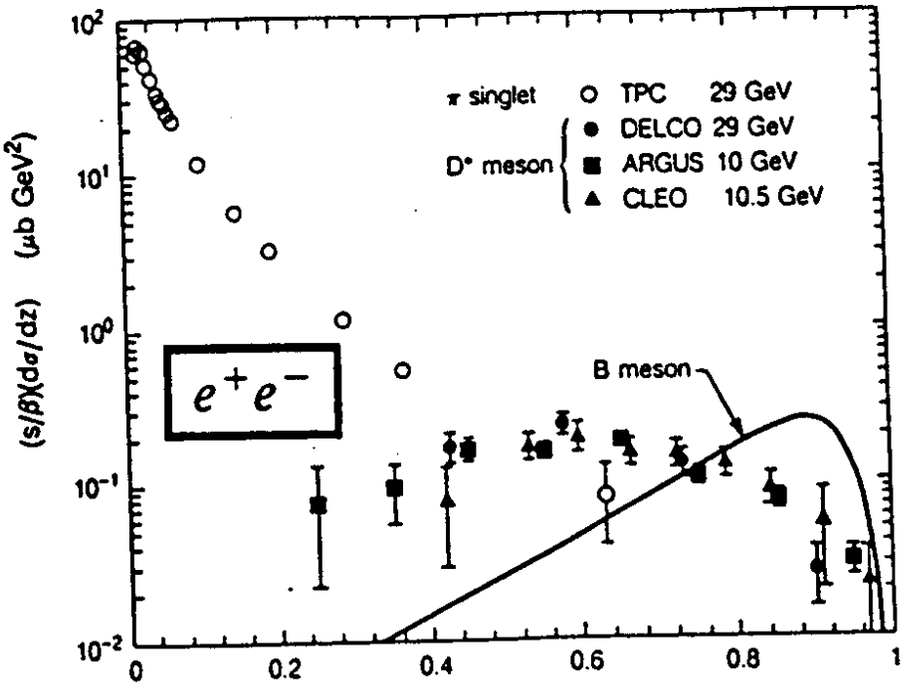

3.7 z distributions of π, D and B mesons . The B-meson curve is a representation of data from various experiments. From the Review of Particle Properties (1986).

part of the diagram is calculated from QCD perturbation theory, the bottom part of the diagram cannot be calculated from perturbation theory and must be taken from experiment.

The $O(\alpha_s)$ terms in the perturbation expansion are drawn in figure 3.8 (there is also a virtual-gluon correction to figure 2.3, which is not shown). In each case, the bottom bubble is not calculable and must be taken from experiment, because it involves long-distance interactions. The upper parts of the diagrams involve a short-distance interaction, so that the appropriate running coupling α_s is small and they may be calculated by a combination of QCD and QED perturbation theory. In figures 3.8a and b the bottom bubbles are just the quark distributions u(x), d(x) .... of §2, but figure 3.8c involves a new function, the gluon distribution in the target nucleon.

Figure 3.8a corresponds to a widening of the forward jet, just like in e^+e^- annihilation. In a small fraction of the events, it yields two separate forward jets. In figure 3.8b, the gluon carries away some of the fractional momentum of the quark, so that the x-value probed by the virtual photon is less than that of the original parton. It turns out that this effect becomes more important with increasing Q^2, so that it makes the plot of F_2 against $1/\omega$ move to the left as Q^2 increases (figure 3.9a). Figure 3.8c generates additional $q\bar{q}$ pairs as Q^2 increases, so that the contribution to F_2 from the sea increases. As the sea contribution is mainly confined to small $1/\omega$ (see figure 2.5), the effect on F_2 is a rise at small $1/\omega$ as shown in figure 3.9b. The combined effect on F_2 is as shown in figure 3.9c.

In practice, the above discussion is qualitatively correct, but a quantitative calculation must take account of contributions

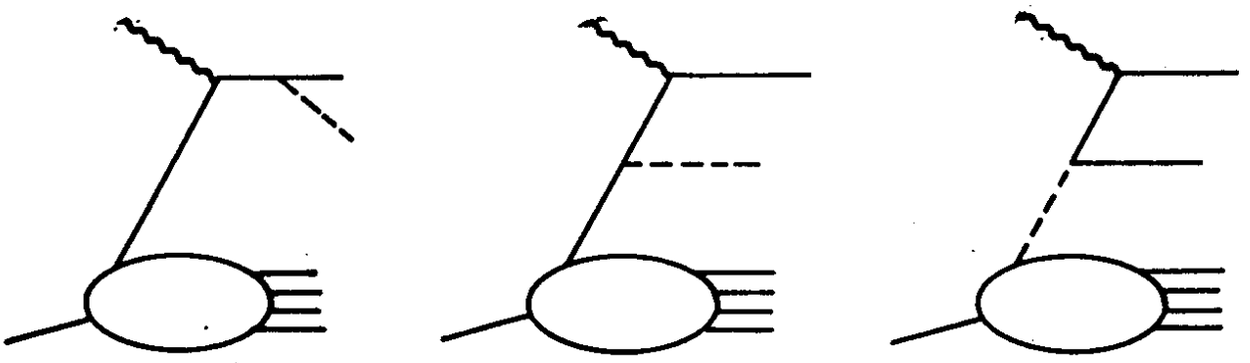

3.8 $O(\alpha_s)$ terms in deep inelastic scattering.

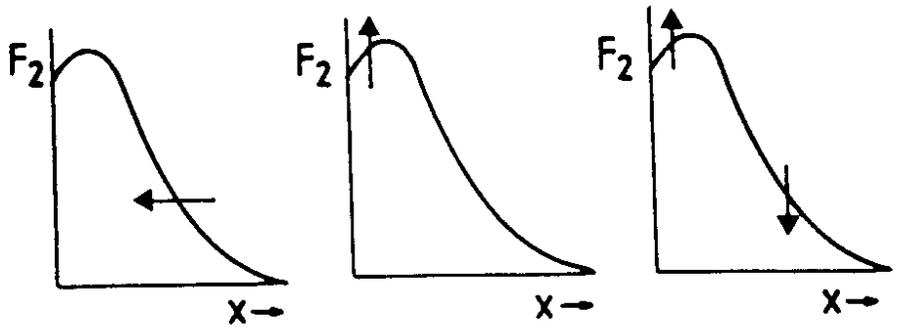

3.9 Variation of F_2 as Q^2 increases: (a) from figure 3.8b, (b) from figure 3.8c, (c) combined effect.

beyond the $O(\alpha_s)$ terms. This is because it turns out that α_s is multiplied by $\log Q^2$. Terms of higher order in α_s, in which more gluons are involved, have correspondingly higher powers of $\log Q^2$. There is an integral equation, the Altarelli-Parisi equation, that enables these to be summed up to all orders of α_s when α_s is multiplied by a large logarithm. This is the leading log approximation (Altarelli, 1982). The resulting behaviour of F_2 as Q^2 increases is still as is shown in figure 3.9c.

As is seen in figure 3.10, the trend in the data is in agreement with this. In order to compare the data with calculation, one has to deal with the "higher-twist" problem. Perturbative QCD predicts logarithmic violation of Bjorken scaling. The higher twists are inverse powers of Q^2, which are relatively negligible at high enough Q^2 but do matter in present data. The European Muon Collaboration (Aubert, 1982) parametrise their effect by multiplying the calculated $F_2(\omega,Q^2)$ by

$$1+\frac{m_o^2}{Q^2}(\omega-1)^{-n} \qquad (3.1)$$

From a fit to their data, they find $m_o \approx 1$ GeV and $n = 2$ (so that the higher twists are very important near $\omega = 1$). The value of m_o is roughly the scale one would expect from a non-perturbative strong-interaction effect such as this.

Gluon effects in the Drell-Yan process

In the Drell-Yan diagram of figure 2.7, the parton momenta k_1 and k_2 are supposed to have small transverse components relative to p_1 and p_2. So $q_T = (k_{1T} + k_{2T})$ is small, at most a few hundred MeV/c in magnitude. However, large values of q_T may be obtained by modifying figure 2.7 to allow gluon radiation as shown in

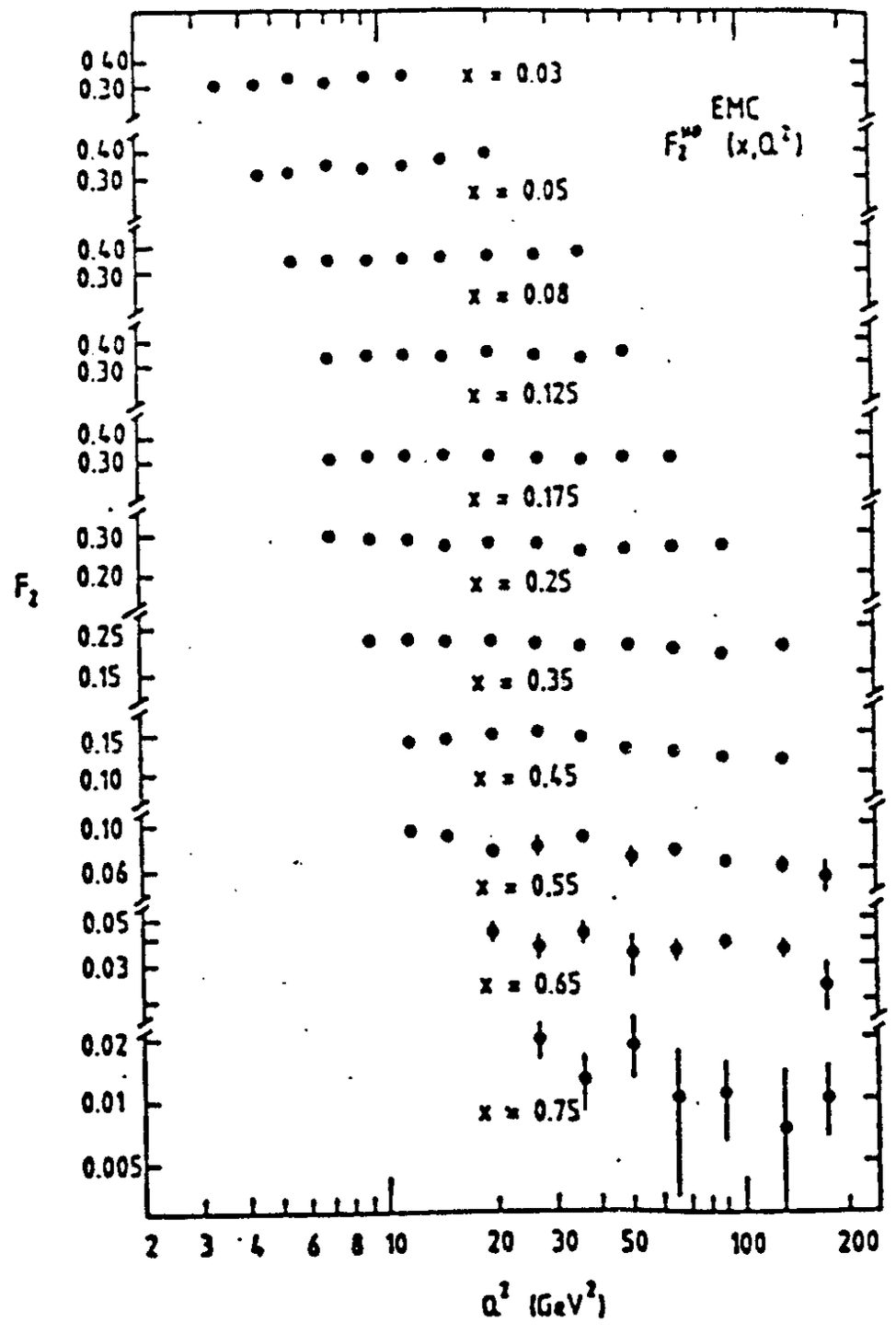

3.10 Data for F_2 , showing breaking of Bjorken scaling.

figure 3.11, where the transverse momentum of the dilepton may be balanced by a gluon jet with the opposite transverse momentum. The central part of the diagram is calculated from perturbation theory, while the upper and lower bubbles must, as always, be taken from deep inelastic lepton scattering experiments. Calculations find that the gluon radiation becomes more important as the incident energy increases, with the consequence that the average transverse momentum of the dilepton (or W) rises. Since a Z decays 20% of the time into a neutrino pair a Z recoiling to a gluon will be seen as a mono-jet. Such gluon radiation effects explain indeed a good fraction of the peculiar mono-jets observed by UA1 (Ellis, Kleiss and Stirling, 1986).

We explained in §2 that, to obtain agreement with experiment, the Drell-Yan formula (2.27) must be multiplied by a factor $K \approx 2.2$. This factor is likely to originate from QCD corrections to figure 2.7. In lowest order the most important diagram is that of figure 3.12, where a virtual gluon is exchanged between the fusing quark and antiquark. Part of the contribution from this diagram is cancelled by other diagrams in which a gluon is radiated, for example figure 3.11. The most important part of what remains is just a constant factor $\frac{\alpha_s}{\pi} \cdot \frac{8}{9}\pi^2$ that multiplies the uncorrected Drell-Yan diagram. Thus if we add together figure 2.7 and figure 3.12, we obtain the correction factor

$$1 + \frac{\alpha_s}{\pi}\frac{8}{9}\pi^2 \qquad (3.2)$$

to the original Drell-Yan formula. It is believed that (3.2) is the beginning of an exponential series, with the higher powers of α_s coming from multigluon corrections to figure 2.7. If this is correct, we have

$$K = \exp\left[\frac{\alpha_s}{\pi} \cdot \frac{8}{9}\pi^2\right] \tag{3.3}$$

In order to get $K \approx 2.2$, we need $\alpha_s \approx 1/4$ which is close to other independent measurements of α_s. The K-factor will decrease as α_s decreases; for W production one might expect $K \approx 1.5$.

This is a very simplified description of what is a very complicated story. For more details, see Altarelli et al. (1978) and Landshoff and Stirling (1982).

Large p_T Hadronic Processes

Consider the reaction

$$pp \to \pi + X \tag{3.4}$$

where, as usual, X denotes a system of hadrons that is not detected. Let the component of the momentum of the pion perpendicular to the line of the colliding beams be p_T. Events in which p_T is small almost surely arise from peripheral collisions, that is those in which only the outer edges of the two colliding protons interact. Because there is no short-distance interaction, the appropriate strong-interaction coupling is not small and one cannot calculate with perturbation theory. In order to be able to use perturbation theory, we need a head-on collision, so that a short-distance interaction occurs. There is no certain way of separating off such (rather rare) events, but intuition suggests that a large-p_T final-state particle should be a good indication of them, and experiment fully supports this.

In order to describe large-p_T data, it is usual to introduce the dimensionless variable

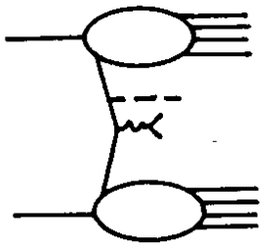

3.11 Gluon radiation in the Drell-Yan process.

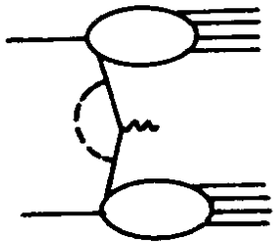

3.12 A QCD correction to the Drell-Yan mechanism.

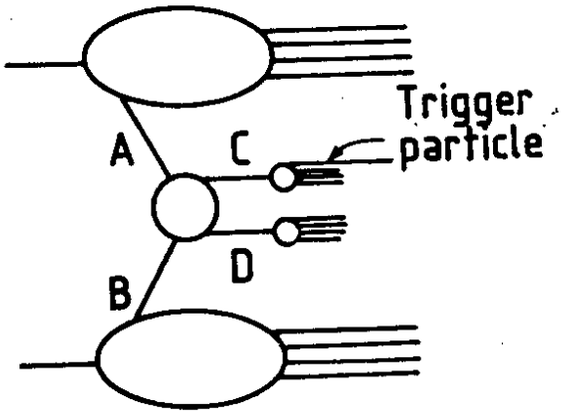

3.13 Hard-scattering models.

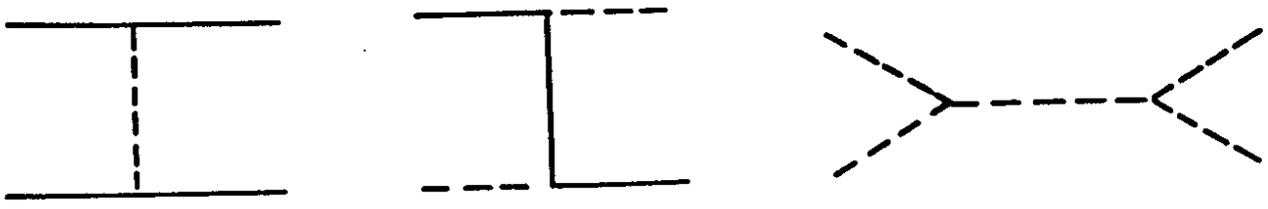

3.14 Examples of the wide-angle scattering A + B → C + D (the solid lines are quarks or antiquarks, and the dashed lines are gluons).

$$X_T = 2p_T/\sqrt{s} \tag{3.5}$$

One may parametrise the data in the form

$$E\frac{d\sigma}{d^3p} = p_T^{-n} F(x_T, \theta) \tag{3.6}$$

where θ is the angle with the initial beam at which the large-p_T pion emerges and where n can be a function of x_T and $\sqrt{s}$. Suppose, however, that as in deep inelastic scattering and in the Drell-Yan process, the dynamics are scale-free, that is no fixed mass or length appears in the function F. Then F must be dimensionless, and in order that the left-hand side of (3.6) may have the correct dimensions we must have $n = 4$. Values of n not far from 4 are found in experiments; n should not be exactly 4 because of scale breaking and other effects.

Calculations of high-p_T reactions use hard-scattering models, figure 3.13. In these models there is a central wide-angle scattering $A+B \rightarrow C+D$, which is calculated from perturbation theory. The objects A,B,C,D can be either quarks or gluons, so the typical lowest-order diagrams for the central wide-angle scatterings are those shown in figure 3.14. The upper and lower parts of figure 3.13 are again the quark, antiquark and gluon distributions in the initial hadrons, which we have already encountered in other processes and cannot be calculated. In figure 3.13 the large-p_T pion is labelled "trigger particle"; it is one of the fragments (almost certainly the fastest) of C, which is either a quark or a gluon jet. The transverse momentum of this jet is balanced by another jet D. Triggering on a single particle at large p_T was used in the ISR experiments which, through the early seventies provided evidence for such jet

effects in hadronic collisions. Nowadays, rather than triggering on a single high-p_T particle, experiments use a calorimeter to trigger on a whole high-p_T jet. The two transverse jets C,D corresponding to figure 3.13 are seen very clearly in experiments at the SPS collider: see figure 1.1.

The agreement between perturbative QCD and experiment is dramatically summarised by figure 3.15 which compares the situation in 1982 and in 1986. In 1982 (Paris conference) first evidence for jet production at the collider had been presented by UA2 and results from UA1 and UA2, as available by the end of 1982, are there compared with QCD predictions. In 1986 (Berkeley Conference) the jet yield can be followed over a tremendous range (9 orders of magnitude in cross section). The 1982 results of 3.15-a correspond to the box in figure 3.15-b and QCD calculations match the data to a very good accuracy (solid line).

It is clear that calculations have to acknowledge uncertainties (K factor....) and one should not claim an accuracy to better than a factor 2 to 3. This is also the limit of the accuracy of the calorimeter measurements in view of the steeply falling yield. This is the present "state of the art" both theoretically and experimentally. Yet the agreement reached over 9 orders of magnitude is impressive.

Figure 3-16 puts together Lego plots for 2 jet, 3 jet and 4 jet events. The study of radiation of extra jets allows one to measure α_s. The value obtained is of the order of 0.2.

Large-momentum transfer Elastic Scattering

Consider the elastic scattering pp → pp at large momentum transfer t. Each of the three quarks in each initial proton

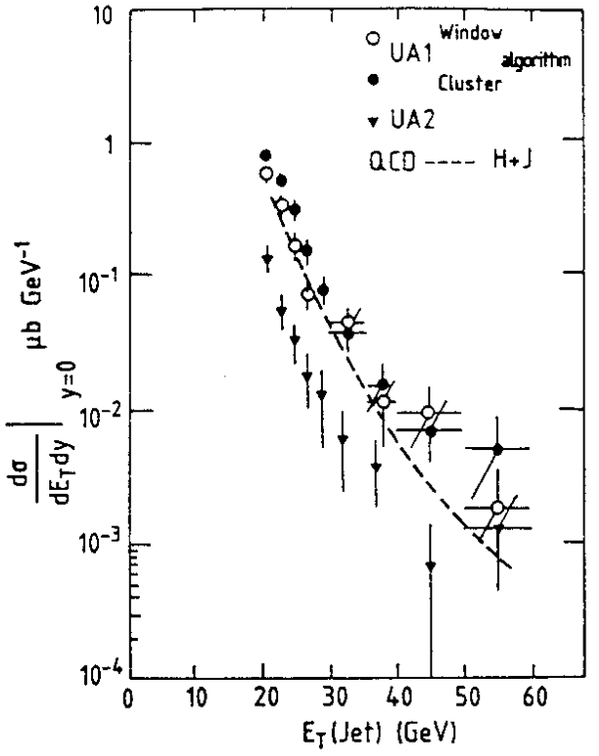

3.15a Inclusive jet production: The experimental situation in 1982 (Collider results) and QCD predictions.

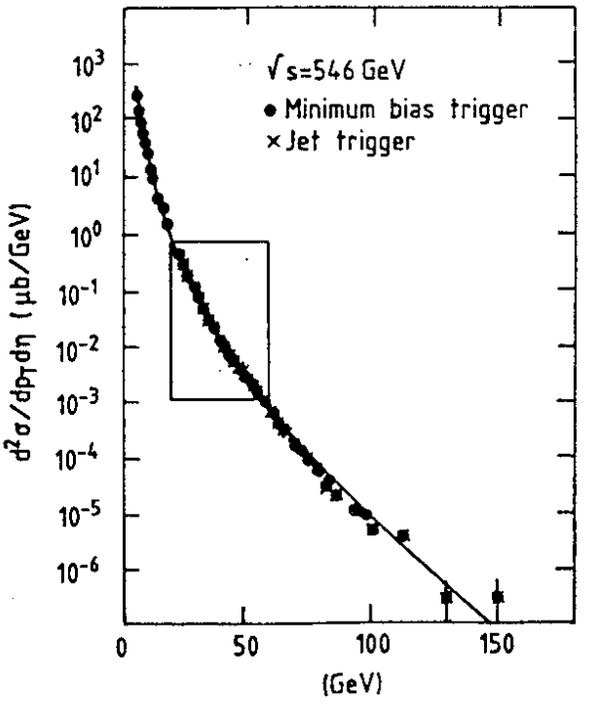

3.15b Inclusive jet production. The present experimental situation and QCD prediction. The box represents the domain spanned by the 1982 data.

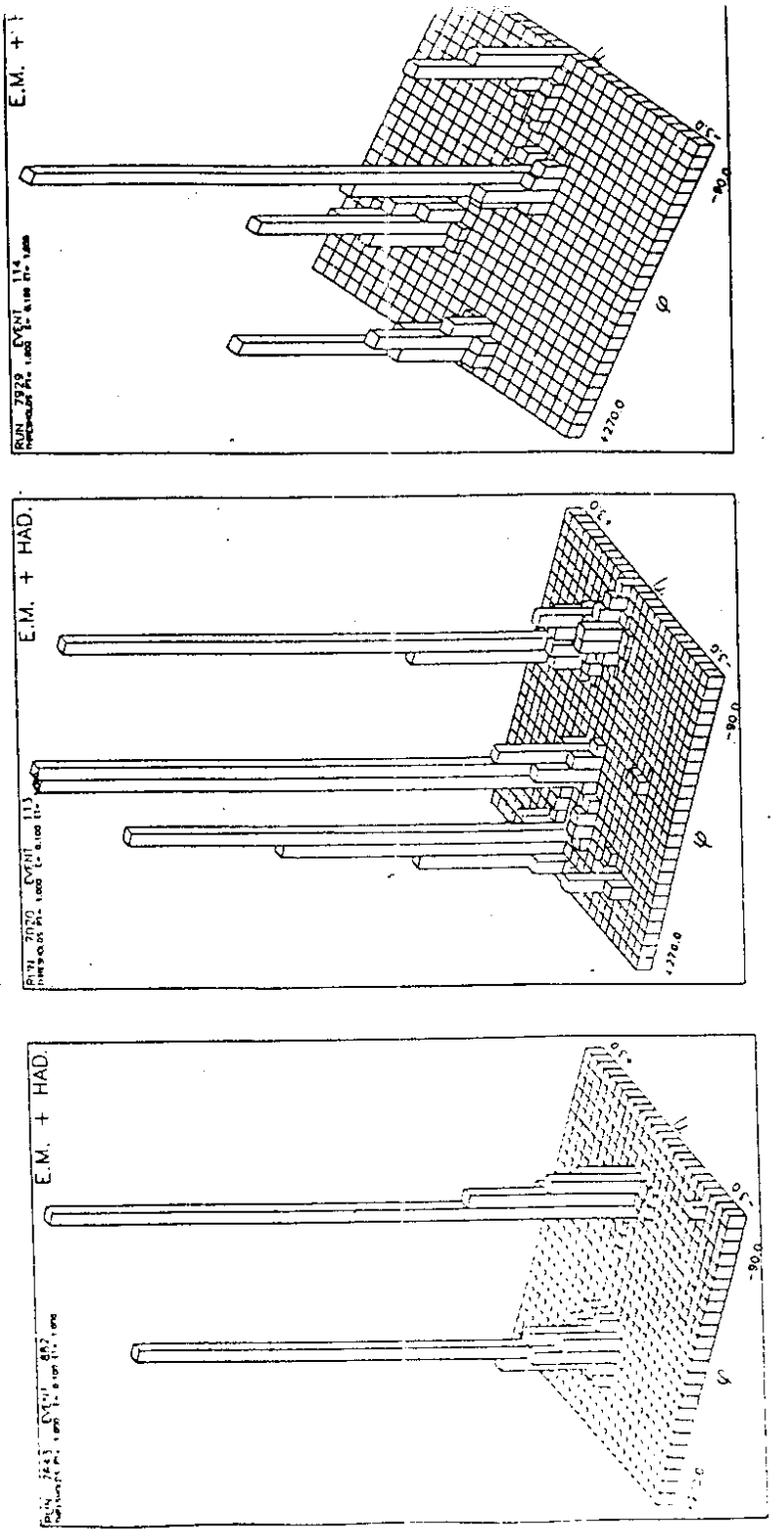

3.1.6 Lego plots (UA1) for 2-jet, 3-jet and 4-jet production.

scatters through wide angle. This is a short distance collision and so may be calculated from perturbation theory; in lowest order the diagram is the first of those in figure 3.14. Putting these three wide-angle quark-quark scatterings together, we obtain the mechanism shown in figure 3.17 for wide-angle elastic pp scattering. At each corner of the diagram there is the proton wave function. Fortunately, we do not need to know much about it in order to calculate how the diagram behaves. For t large compared with the proton mass, though much less than s, we find (Donnachie and Landshoff, 1979)

$$\frac{d\sigma}{dt} = Ct^{-8} \qquad (3.7)$$

where C is an energy-independent constant, which in principle can be calculated in terms of the wave function and α_s. The form (3.7) is compared with high-energy data in figure 3.18. This successful comparison between theory and experiment was the first confirmation that gluons have spin 1; spin 0 gluons would give $s^{-6}t^{-2}$ instead of t^{-8}.

We have so far discussed QCD in a very "low-brow" way focussing on some specific effects and calculations to lowest order in α_s. We do not wish to leave the subject without discussing also how complicated calculations become when considering higher order effects.

Renormalisation

Quantum field theories are plagued with infinities. In some cases, these infinities can be explained away, and then the field theory is said to be renormalisable. QCD holds the unique position that it is the only renormalisable field theory that is a

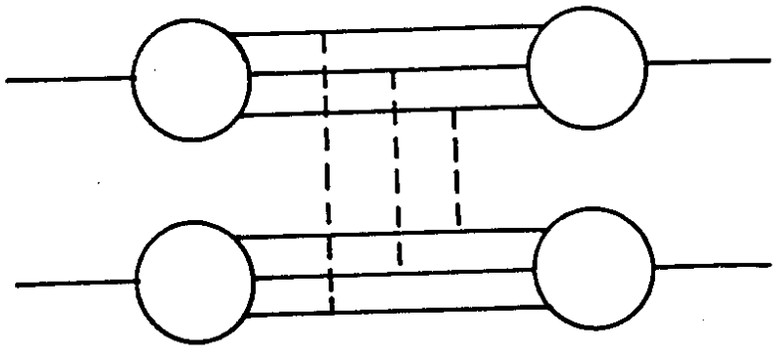

3.17 Mechanism for large t elastic scattering.

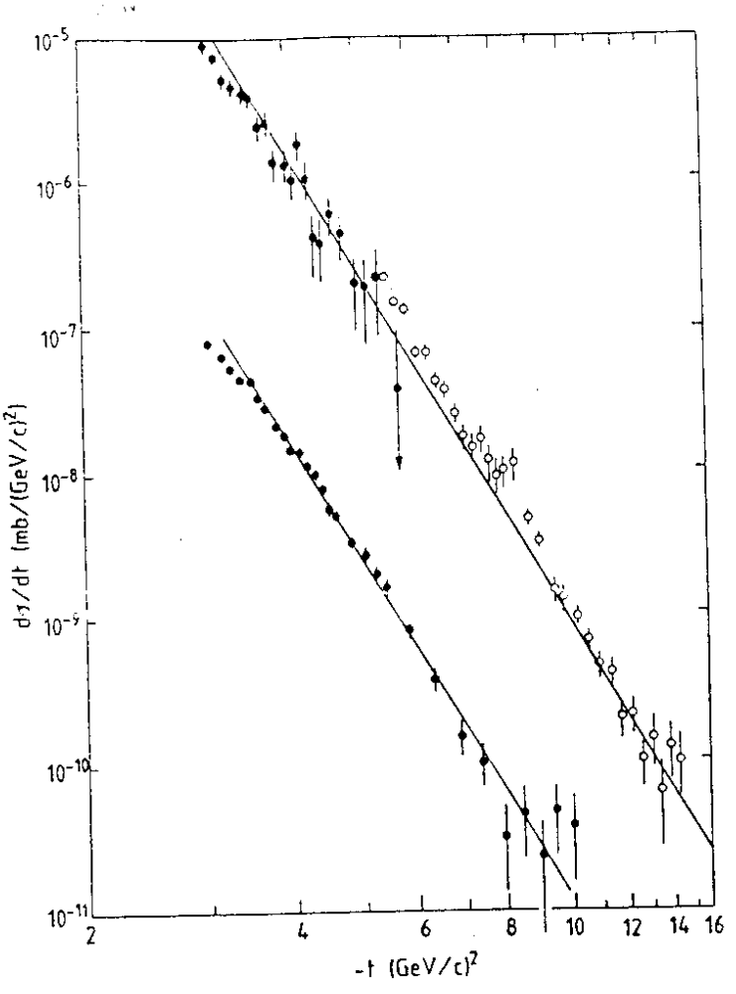

3.18 pp elastic scattering data at various FNAL and ISR energies. The lower data have been divided by 100; in each case the straight line is Ct^{-8} with $C = 0.09$ mb$(GeV)^6$.

plausible candidate for describing the strong interactions.

Renormalisation is a big and difficult subject: see the book by Collins (1984). The basic idea is as follows. When one develops a perturbation expansion, one first divides the Hamiltonian into a "free" part H_o and an "interaction" part H_I:

$$H = H_o + H_I$$

The renormalisation procedure amounts to a rearrangement of H; one removes an infinite term Δ from H_I and includes it in H_o:

$$H = (H_o + \Delta) + (H_I - \Delta) \qquad (3.8)$$

The calculation now regards $(H_o + \Delta)$ as the free part of H, and $H_I - \Delta$ as the interaction. The term Δ is chosen so as to make the results of calculations finite and physically meaningful. However, this does not provide a unique prescription for choosing Δ. Different choices correspond to different "renormalisation schemes". In a renormalisable theory, the values of physical quantities are the same in all renormalisation schemes, <u>provided</u> that they are calculated without any approximation being made, which means to all orders. But in practice one cannot avoid making an approximation, and then the choice of renormalisation scheme can greatly affect the answer to the calculation.

The original free part H_o of H contains a mass for each quark in the theory. The rearrangement (3.8) changes, or renormalises, these masses by the addition of "counter terms" whose structure is the same as that of the original mass terms. Likewise, it renormalises the coupling g in the interaction part of H.

In the unrenormalised Lagrangian, the gluon has no mass, and one can show that, because of the gauge invariance, this remains true after renormalisation. One often sets the quark masses to zero also: this enforces chiral symmetry but calculations whose answer depends on the quark mass are usually not valid. Infrared divergences may not be properly cancelled then and this is liable to be a signal that perturbation theory cannot after all be used. If the quark masses are zero before renormalisation, the Lagrangian is chiral invariant and one can show that this implies that the renormalisation keeps them zero. The theory has no mass scale. However, the coupling-constant renormalisation introduces a mass μ into the theory.

For example, in the MOM (momentum subtraction) renormalisation scheme, μ is defined such that near $k^2 = \mu^2$ each propagator carrying momentum k has the same form after renormalisation as before. Changing the choice of μ changes the value of the renormalised coupling g, so that effectively g is a function of μ. For this reason, it is called a "running coupling". There is an equation, the renormalisation group equation, that relates the values of g at different values of μ. We usually work with $\alpha_s = g^2/4\pi$, and for $\mu^2 \gg \mu_o^2$ the equation gives

$$\alpha_s(\mu^2) = \frac{1}{\left[\alpha_s(\mu_o^2)\right]^{-1} + \beta_o \log \mu^2/\mu_o^2}$$

$$\beta_o = \frac{33 - 2N_f}{12\pi} \qquad (3.9)$$

where N_f is the number of quark flavours. Provided that $N_f \leqslant 16$, the coefficient multiplying the logarithm is positive and $\alpha_s(\mu^2)$ decreases as μ^2 increases: this is asymptotic freedom. One can

trace the positive character of the first term to the effect of virtual longitudinally polarised gluons, whereas transverse gluons give the same sign as quarks.

It is usual to define

$$\Lambda^2 = \mu_o^2 \exp\left[-1/\beta_o \alpha_s(\mu_o^2)\right] \tag{3.10}$$

so that

$$\alpha_s(\mu^2) = \frac{1}{\beta_o \log \mu^2/\Lambda^2} \tag{3.11}$$

The value of the fixed mass Λ cannot be calculated: we have to extract it from experiment.

In other renormalisation schemes, μ is defined in a different way and the function $\alpha_s(\mu^2)$ is different. However, for $\mu \gg \Lambda$ the form (3.11) is always valid, but with the value of Λ depending on the scheme. A scheme that is frequently used is $\overline{\text{MS}}$ (modified minimal subtraction), with

$$\Lambda_{\overline{\text{MS}}} \approx \tfrac{1}{2}\Lambda_{\text{MOM}} \tag{3.12}$$

Experiment finds that the value of $\Lambda_{\overline{\text{MS}}}$ is about 150 MeV.

Consider two different schemes, with couplings $\alpha_1(\mu^2)$ and $(\alpha_2(\mu^2)$. Then

$$\alpha_1(\mu^2) = \frac{\beta_o}{\log \mu^2/\Lambda_1^2}, \qquad \alpha_2(\mu^2) = \frac{\beta_o}{\log \mu^2/\Lambda_2^2} \tag{3.13}$$

For $\mu \gg \Lambda_1, \Lambda_2$ we may expand α_2 in powers of α_1:

$$\alpha_2(\mu^2) = \frac{\beta_0}{\log \frac{\mu^2}{\Lambda_1^2} - \log \frac{\Lambda_2^2}{\Lambda_1^2}}$$

$$= \frac{\beta_0}{\log \frac{\mu^2}{\Lambda_1^2}} \left[1 + \frac{\log \Lambda_2^2/\Lambda_1^2}{\log \mu^2/\Lambda_1^2} + \ldots \right]$$

$$= \alpha_1(\mu^2) \left[1 + \frac{\log \Lambda_2^2/\Lambda_1^2}{\beta_0} \alpha_1(\mu^2) + \ldots \right] \qquad (3.14)$$

So a change of renormalisation scheme has the effect

$$\alpha_s \to \alpha_s \left[1 + A\frac{\alpha_s}{\pi} + \ldots . \right] \qquad (3.15)$$

where A is a constant. it is straightforward to see from (3.11) that changing the renormalisation scale μ has a similar effect.

Suppose now that some physical quantity P has been calculated in some scheme with a given choice of renormalisation scale, giving the result

$$P = B\alpha_s^N \left[1 + C\frac{\alpha_s}{\pi} + \ldots . \right] \qquad (3.16)$$

where B and C are constants or functions of the variables in the problem. If we change either the scheme or the scale, (3.15) gives

$$P \to B\alpha_s^N \left[1 + (C + NA)\frac{\alpha_s}{\pi} + \ldots \right] \qquad (3.17)$$

The statement that the theory is renormalisable implies that the sums of the infinite series (3.16) and (3.17) are equal. However, in practice one does not calculate the full infinite series; one truncates it after just a few terms, maybe even after the first term. The truncated series are not equal.

When one truncates the series, throwing away an infinite number of terms after the first few, one implicitly assumes that this introduces only a small error. The question then arises: in what scheme, and for what value of the renormalisation scale, is this a good approximation? Because one has not calculated the terms that have been discarded, this question cannot be answered, except by guesswork.

Often, one just compares the first term with experiment, $P = B\alpha_s^N$. One is then implicitly assuming a renormalisation scheme that makes the rest of the series negligible. One cannot identify this scheme, beyond saying that it is the one appropriate for a leading-order calculation of the quantity P. The comparison with experiment yields a corresponding Λ, $\Lambda_{L.O.(P)}$ say. If one now goes through the same procedure for some other physical quantity P', the result will be another Λ, $\Lambda_{L.O.(P')}$. There is no reason to expect that $\Lambda_{L.O.(P)} = \Lambda_{L.O.(P')}$.

If two terms are calculated in P,

$$P = B\alpha_s^N \left\{1 + C\frac{\alpha_s}{\pi}\right\} \qquad (3.18)$$

it is often assumed that it is valid to compare this with experiment if $|C| \ll 1$. This is based on the hope that the other terms, not calculated, will then also have small coefficients. But,

because the other terms have not been calculated, this cannot be more than a hope.

Much has been written about the problem of how to choose the renormalisation scheme and scale, but the problem remains unsolved, and will surely remain so. In practice, rather few processes have been calculated beyond non-leading order, because such calculations demand a great deal of work and computing power. In these circumstances, one may as well choose the $\overline{\text{MS}}$ scheme, for lack of any guidance as to which is best, and choose as the value of μ some scale obviously associated with the quantity being calculated. But one must accept that our lack of knowledge imposes limitations on the numerical accuracy that we can reasonably expect.

In spite of this, the successes of perturbative QCD are impressive. At the qualitative level there is, for example, the prediction and discovery of the third jet in e^+e^- annihilation. The calculation of, for example, the cross-section for jet production in $p\bar{p}$ collisions may be only semi-quantitative because of the difficulties we have described, but as previously said one can safely say that theory and experiment agree within a factor of about 3 as the cross-section varies through some 9 orders of magnitude! Better accuracy will require more powerful computing facilities on the theoretical side, and more sophisticated calorimetry in the experiments.

The present success of QCD originates from the beauty of the theory (despite ugly computational difficulties which we have stressed) and an impressive amount of semi-quantitative successes with many different phenomena. It is a powerful way to approach all hard processes.

We may say that we thus understand the structure of matter at the level of 10^{-17}m and beyond. What about physics at the scale of hadronic sizes, namely 10^{-15}m? This is what we now turn to.

4. SOFT HADRONIC REACTIONS

Structure of Typical Events

It has been stressed that only a very small fraction of hadronic interaction events involve the head-on collision that is necessary for perturbative QCD to be applicable. In this section we describe the phenomenology of the other events, which make up nearly all of the total cross-section.

A typical event at the SPS Collider has about 30 charged particles, (50 particles in total). The particles emerge in two longitudinal jets, that is jets travelling in the directions of the colliding beams. The average transverse momentum of the particles in these jets is a few hundred MeV/c; it rises only very slowly with the incident centre-of-mass energy $\sqrt{s}$. Plots of the longitudinal-momentum distribution are commonly made against a variable y known as rapidity:

$$y = \tfrac{1}{2} \log \frac{E + p_L}{E - p_L} \qquad (4.1)$$

where E, p_L are the energy and longitudinal momentum of the final-state particles. The rapidity has the property that it changes in a very simple way under a Lorentz boost along the direction of the colliding beams: $y \to y +$ constant. A related variable is the pseudorapidity η:

$$\eta = -\log \tan \tfrac{1}{2}\theta = \frac{1}{2} \log \frac{p + p_L}{p - p_L} \qquad (4.2)$$

where θ is the angle between the particle's momentum vector and one of the incident momenta. For momenta large compared with the

particle mass, $\eta \approx y$, so rapidity may be measured without a momentum measurement.

Plots of pseudorapidity distributions at various high energies are shown in figure 4.1. The variable along the horizontal axis is the difference between the particle's pseudorapidity and its maximum value possible. The particles that have rapidity within about 2 units of the maximum possible may be regarded as fragmentation products of the initial beam; their distribution depends on what is the beam particle and it varies rather little with the incident energy. In order to examine this part of the plot in more detail, one often uses instead of $y(\eta)$ the Feynman variable

$$x_F = p_L/p_L^{max} \qquad (4.3)$$

In terms of this variable, the beam fragmentation region is $0 < x_F < 1$, while the remainder of the distributions shown in figure 4.1 correspond to very small x_F. Figure 4.1 shows only half the rapidity plot; at each energy the left-most data point is at half the maximum possible value of the rapidity difference $(y^{max} - y)$. The full plot would show the fragmentation region of the other initial beam particle occupying about 2 units of rapidity on the left of the plot.

The region of the rapidity plot between the two fragmentation regions is called the central region. As is seen in figure 4.1, the number density of particles in the central region rises slowly with the initial energy. The central region is independent of the identities of the initial colliding particles: it results somehow from the production of $q\bar{q}$ pairs as the tube of

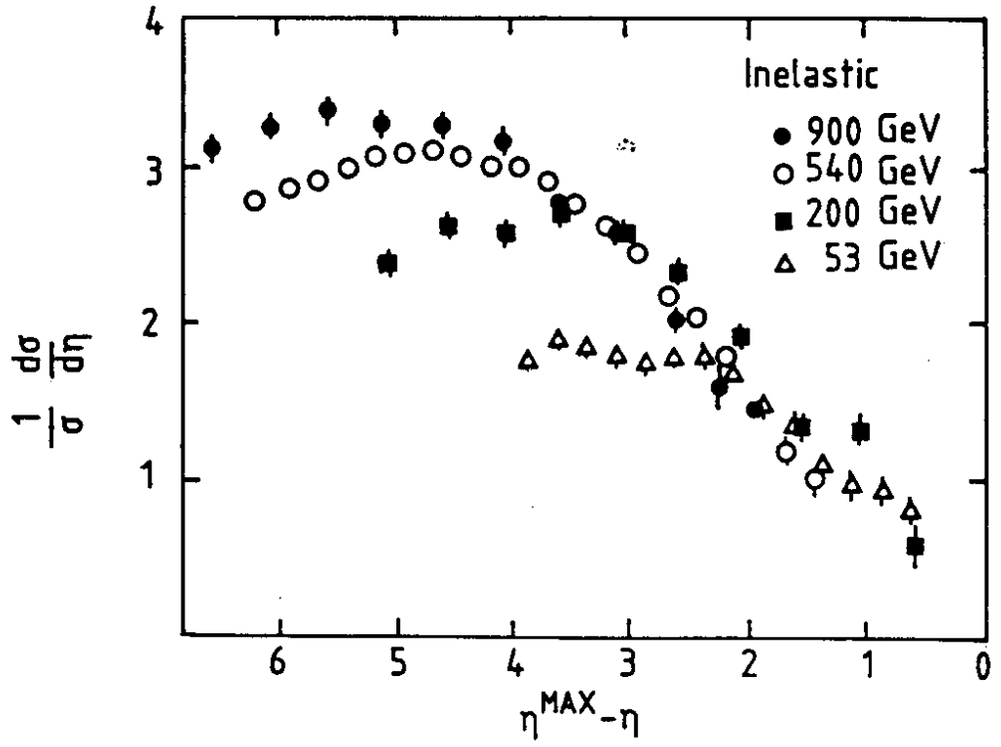

4.1 Pseudorapidity distributions of particles produced in collisions at the ISR and the Collider (Rushbrooke, 1985). At each energy, only half the plot is shown.

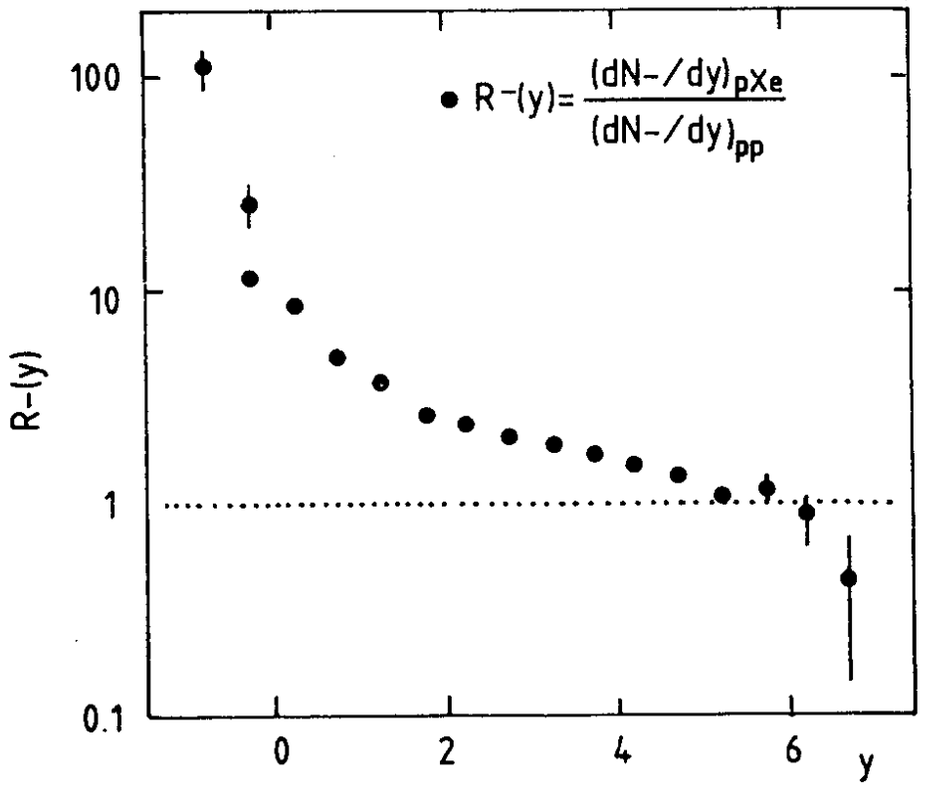

4.2 Multiplicity distributions in p Xe collisions, compared with pp collisions (Faessler, 1984).

colour flux associated with the quarks in the initial hadrons stretches when they pass one another. The details of the dynamics are not well understood. Nor are the details of the dynamics of the particle production in the fragmentation regions, though it is well established that quarks are somehow involved (Pauss et al., 1985).

There is a further region of the rapidity plot, the diffractive region, which is not explicit in figure 4.1 because it corresponds to particles going down the beam pipes. It is at the extreme right of the rapidity plot, $y \approx y^{max}$, that is x_F close to 1. It corresponds to the initial beam particle scattering quasi-elastically instead of fragmenting. We will consider it later in this section.

Nuclear-target Effects

When a fast hadron enters a nucleus, one might have expected there first to be a collision with one of the nucleons, producing several fast hadrons. These could then collide with other nucleons, and in turn produce further fast hadrons. However, this cascading effect is not observed at high energy. Figure 4.2 shows the rapidity distribution of negative particles produced in proton-xenon collisions, divided by that from pp collisions: the ratio at large rapidity is not much greater than 1.

Several possible explanations of this exist (Busza, 1976). A simple one, which has come to play an important role in the theory of quark plasma physics, is that it is the valence quarks of the beam particle that are responsible for producing the fast hadrons. It is assumed that, after a valence quark first interacts, a certain time must elapse before it can materialise as a jet of hadrons. This formation time is of the order of 1 fm

in the rest frame of the quark. If the quark is moving fast, it has emerged from the nucleus before the formation time has elapsed, so that all that happens to it within the nucleus is that it scatters quasi-elastically on any further nucleons it encounters. Since the hadron formation takes place after the quark has passed through the nucleus, the multiplicity is almost the same as for a proton target. Of course, this argument applies only to the beam fragmentation region of the rapidity plot. As is seen in figure 4.2, in the target fragmentation region things are very different. There is plenty of time for rescattering effects to take place in that case!

Regge Theory

Consider bound states of a quark and an antiquark, or of three quarks, with a given flavour wave function but different orbital angular momenta. That is, fix the baryon number, isospin, strangeness and charge parity but not the spin. If one plots the spin α against the square of the mass, one obtains families of straight lines, known as Regge trajectories. An example is shown in figure 4.3. This figure actually contains both I = 0 and I = 1 mesons and both charge parities, that is there are four very nearly coincident Regge trajectories. The straight line has equation

$$\alpha(M^2) = 0.44 + 0.93 M^2 \qquad (4.4)$$

The latest edition of the Review of Particle Properties (1986) lists also isospin 1 mesons of spins 4, 5 and 6, and isospin 0 mesons of spins 5 and 6. They also lie approximately on the line (4.4), though their existence awaits further experimental evidence before it can be confirmed.

Such a linear rise of α with M^2 of course would follow from a model in which a quark and an antiquark rotate at the speed of light joined together by an elastic string. The slope α' is related to the string tension.

If one extrapolates $\alpha(M^2)$ down to negative values of M^2, so that now M^2 may be regarded as a momentum transfer t, it may be used to calculate the high-energy behaviour of scattering amplitudes. This is the result of a well-established theory and has been well tested by experiment (Collins, 1977). This Regge theory calculates the combined effect of the exchange of all the particles on a given trajectory α (see figure 4.4); their contribution to a scattering amplitude T at high energy $\sqrt{s}$ is

$$T(s,t) = \beta(t)\, s^{\alpha(t)}\, (e^{-i\pi\alpha(t)} + C) \qquad (4.5)$$

Here, $\beta(t)$ is a function that cannot be calculated, but it is known to be real. The last factor is called the signature factor; it determines the phase of the contribution to the amplitude ($C = \pm 1$ is the charge parity of the trajectory). Thus the trajectory determines both the energy variation and the phase of the amplitude.

Regge theory played the central role in hadron physics research during the 1960's. It had many successes. Work on it came to an end partly because the successes of QCD at short distances attracted full attention and partly because it was realised that, to improve on the theory, it was necessary to correct it by including contributions corresponding to the simultaneous exchange of several Regge trajectories. More accuracy was only achieved at the price of extra complications involving new parameters. Even now, we do not know how to do this properly, but it

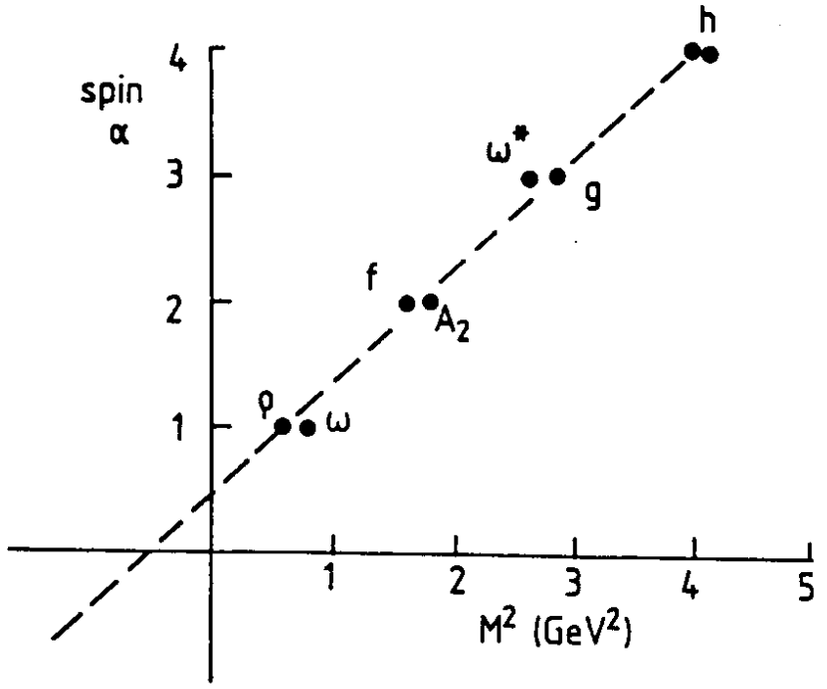

4.3 Coincident Regge trajectories for mesons.

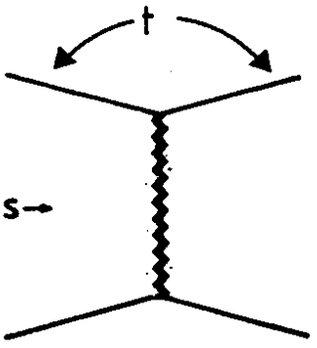

4.4 Exchange of a set of particles on a given Regge trajectory.

is amusing to note that attempts to learn how led to the development of today's superstring theory.

The Pomeron

If one neglects the simultaneous exchange of more than one trajectory, one must still add together separate contributions from all the single trajectories that have the right quantum numbers to be exchanged in the given amplitude. In an elastic-scattering amplitude one can obviously exchange the quantum numbers of the vacuum, B = I = S = 0, C = + 1. At high energy, such a trajectory is found to be enough to explain most of the elastic scattering at small t. Because of the optical theorem,

$$\sigma^{Tot} = \frac{1}{s} \mathrm{Im}\, T(s,t = 0), \qquad (4.6)$$

it also accounts for most of the total cross-section. The trajectory is called the pomeron trajectory, after the Soviet physicist Pomeranchuk.

It is not understood what the pomeron trajectory is. No particle lying on it has yet been identified. The lowest spin of such a particle would be 2, and its mass would be in the region of 2 GeV. Any such particle is likely to be a glueball.

The reason for this is that the pomeron is believed to correspond to the exchange of a number of gluons (at least two, in order to achieve the vacuum quantum numbers). The theory of this is not understood, and we should not expect it to be, because we are dealing with the long-range strong interaction, for which we cannot use perturbation theory.

In order to account for the data for σ^{Tot} and elastic

scattering, we take the pomeron trajectory to be linear like the other trajectories:

$$\alpha_p(t) = 1 + \epsilon + \alpha' t \qquad (4.7)$$

In order to describe the rise of σ^{Tot} at high energy we need (Collins and Gault, 1982) ϵ to be about 0.09, while the very-small-t pp and $\bar{p}p$ elastic data require $\alpha' = 0.25\ GeV^{-2}$. In figure 4.5 are shown data for pp and $\bar{p}p$ total cross-sections. Their difference is well accounted for by the exchange of the ρ and ω trajectories. According to (4.4), (4.5) and (4.6) this predicts an energy variation like $s^{-0.56}$, and the curves obey

$$\sigma(\bar{p}p) - \sigma(pp) = 70\, s^{-0.56} \qquad (4.8)$$

The average of the pp and $\bar{p}p$ cross sections initially falls with increasing energy; this is due to f and A_2 exchange, which again behaves like $s^{-0.56}$. The rise at higher energy is due to pomeron exchange:

$$\tfrac{1}{2}\left[\sigma(\bar{p}p) + \sigma(pp)\right] = 22.7\, s^{0.08} + 105\, s^{-0.56} \qquad (4.9)$$

Single-pomeron exchange behaves like s^{ϵ}, where ϵ is defined in (4.7). Actually, ϵ is a little greater than .08, but in the first term of (4.9) there is included a contribution from the exchange of two pomerons. We do not know how to calculate this properly, but we do know that its contribution to σ^{Tot} is negative. At Collider energy it is about 10% of the total (Donnachie and Landshoff, 1986), but it becomes more important at higher energy. The single power $s^{0.08}$ is only an approximate representation.

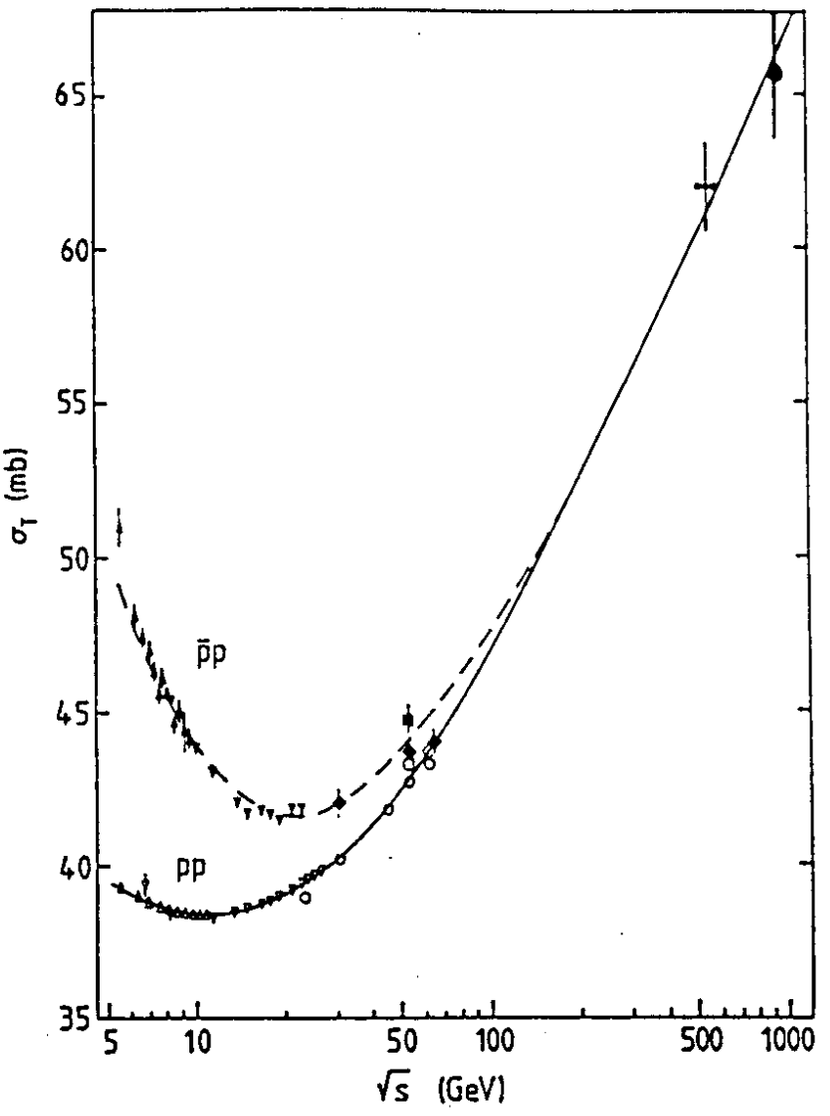

4.5 Data for pp and $p\bar{p}$ total cross sections. The calculated curves are from Donnachie and Landshoff, 1986.

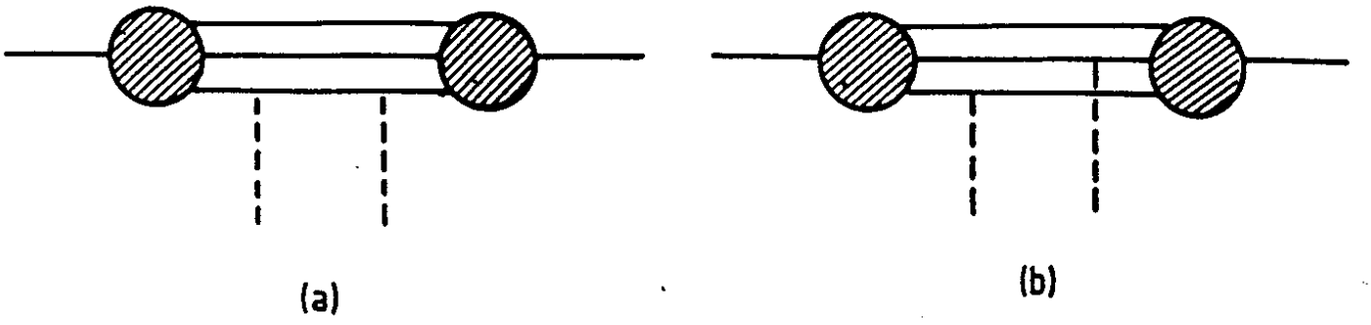

4.6 Couplings of two gluons to a nucleon.

The pomeron has a surprising property, which is actually quite hard to understand in the gluon exchange picture: it couples to just one quark in a hadron. If the pomeron is two or more gluons, it is not clear why each of the gluons should couple to the same quark. If figure 4.6a is allowed, why not also figure 4.6b? First evidence that only one quark is involved came from the additive-quark rule for total cross sections. This rule says that one can calculate the cross section for the scattering of two hadrons by summing the cross-sections for the possible separate scatterings of their valence quarks (and antiquarks). The rule is experimentally correct to within 10%, and probably rather better if one applies it only to the part of the cross section that arises from pomeron exchange (though we cannot extract this accurately from the data).

Elastic Scattering

The conclusion, then, is that the pomeron couples to a single quark, and counts the number of quarks in a hadron. This is rather like the photon. Suppose we assume (Landshoff and Polkinghorne, 1971; Donnachie and Landshoff, 1986) that it behaves just like the photon, except of course that its quantum numbers are $I = 0$, $C = +1$. Then when we calculate elastic scattering of a proton or an antiproton, we take care of the bound-state effects by introducing the Dirac elastic form factor $F_1(t)$. So the contribution from single-pomeron exchange is

$$\frac{d\sigma}{dt} = \frac{\left[3\beta_0 F_1(t)\right]^4}{4\pi} s^{2\alpha_p(t)-2} \qquad (4.10)$$

Here, $\alpha_p(t)$ is the pomeron trajectory (4.7). The constant β_0 is the analogue for the pomeron coupling of the electric charge; its

magnitude is already fixed by the fit to the total cross sections. The 3 appears because the proton has 3 valence quarks. The Dirac form factor $F_1(t)$ is the isoscalar form factor; it is extracted from data for the average of ep and en elastic scattering. (There are normally two Dirac form factors, but the other one is very small in the isoscalar combination). Figure (4.7) shows the comparison between (4.10) and experiment. The formula fits equally well throughout the ISR energy range, and also to small-t pd elastic scattering, if one makes use of the elastic form factor of the deuteron measured in ed scattering.

Diffraction Dissociation

Consider now events in which one of the incident particles is scattered quasi-elastically and loses very little of its momentum, that is it emerges from the reaction with x_F close to 1. The other initial particle breaks up into a system of hadrons, of invariant mass M, which is well separated in rapidly from the first incident particle. These events are called diffraction-dissociation events; they are thought to arise from pomeron exchange: see figure 4.8. There is an obvious resemblance between figure 4.8 and figure 2.1, and if indeed the pomeron behaves like an isoscalar photon the connection is quantitative (Jaroskiewicz and Landshoff, 1974; Donnachie and Landshoff, 1984). We find that

$$s\frac{d^2\sigma}{dt\,dM^2} = \frac{\beta_o^4\,[3F_1(t)]^2}{4\pi}\left(\frac{M^2}{s}\right)^{1-2\alpha_p(t)}\bar{F}_2 \qquad (4.11)$$

Here, $\bar{F}_2$ is a combination of quark distribution functions, just like (2.14) except that the squares of the quark charges do not appear. It is a function of $Q^2 = -t$ and $\omega = 1/x \approx M^2/Q^2$. From

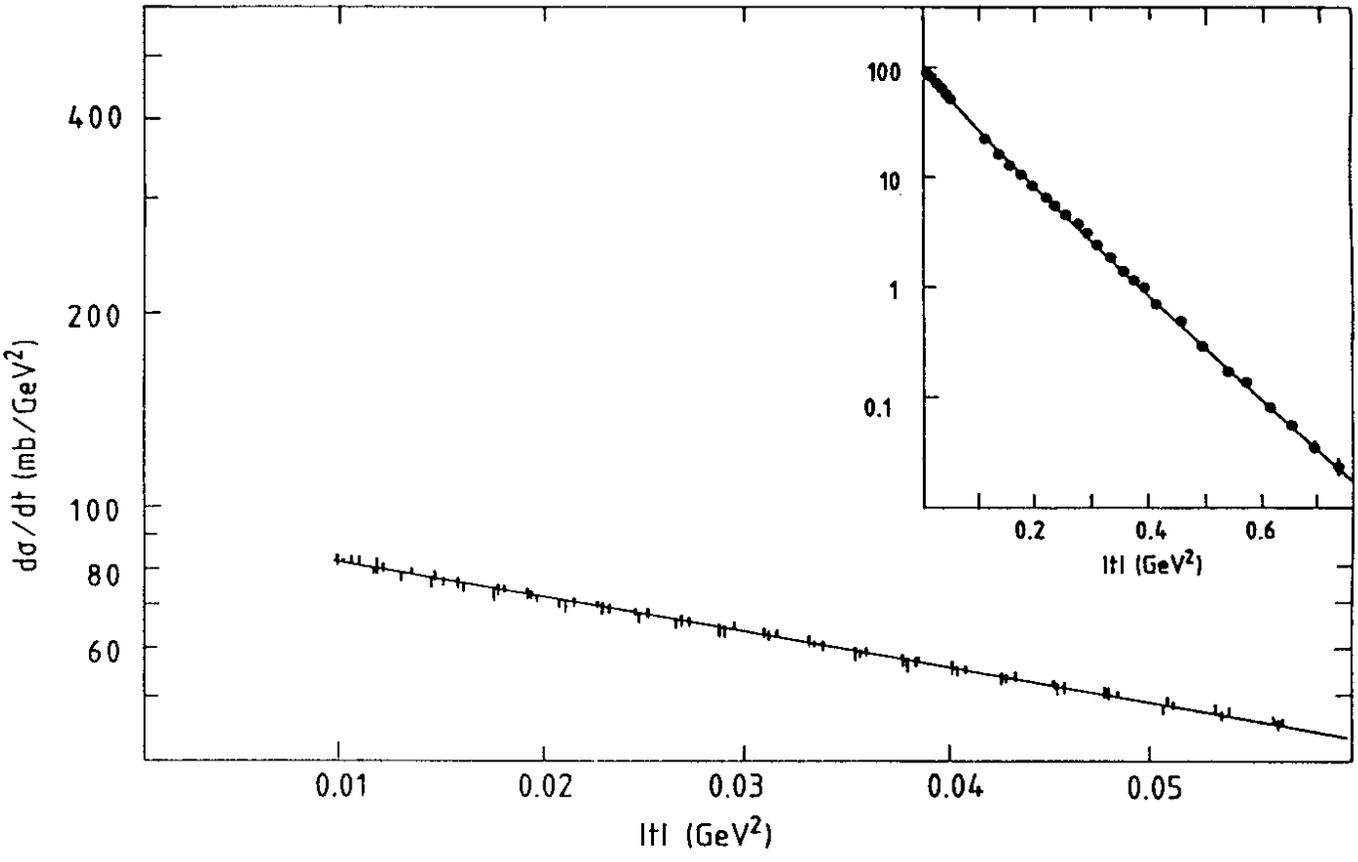

4.7 ISR data for pp elastic scattering. The curves correspond to (4.10) with $\alpha' = 0.25\ (\text{GeV})^{-2}$.

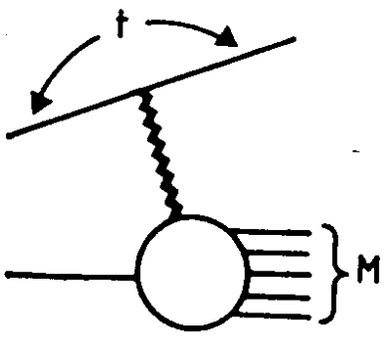

4.8 Diffraction dissociation, by pomeron exchange.

simple kinematics,

$$\frac{M^2}{s} = 1 - x_F \qquad (4.12)$$

so that the diagram of figure 4.3 and the formula (4.11) are applicable for $M^2 \ll s$. All the quantities in (4.11) have been determined from other experiments, though the deep inelastic lepton scattering data have to be extrapolated to the values of Q^2 and ω required here. The result is shown in figure 4.9, together with data from the ISR and the SPS Collider.

Experiments on diffraction dissociation are continuing. A recent result from an ISR experiment (Smith et al., 1985) is that the pomeron interacts with a single quark in the target hadron and knocks it out, in the same way as a quark is knocked out when it absorbs the virtual photon in deep inelastic muon scattering (figure 2.3). The UA8 Collaboration at the SPS Collider is looking for events where the system M of hadrons in figure 4.8 contains a pair of high-p_T jets. Just as in hadron-hadron collisions the rate for high-p_T jet production is calculated using the quark and gluon distributions in the initial colliding particles, so here it will depend on those in the colliding pomeron and nucleon. So the data will give information about the structure of the pomeron.

In all these soft processes QCD is presently used more as a framework than as an actual theory. The regularities met speak for some deep simplicity still to be unravelled.

Minijets

An interesting topic whose experimental study is just beginning is that of minijets. The physics of these is at the

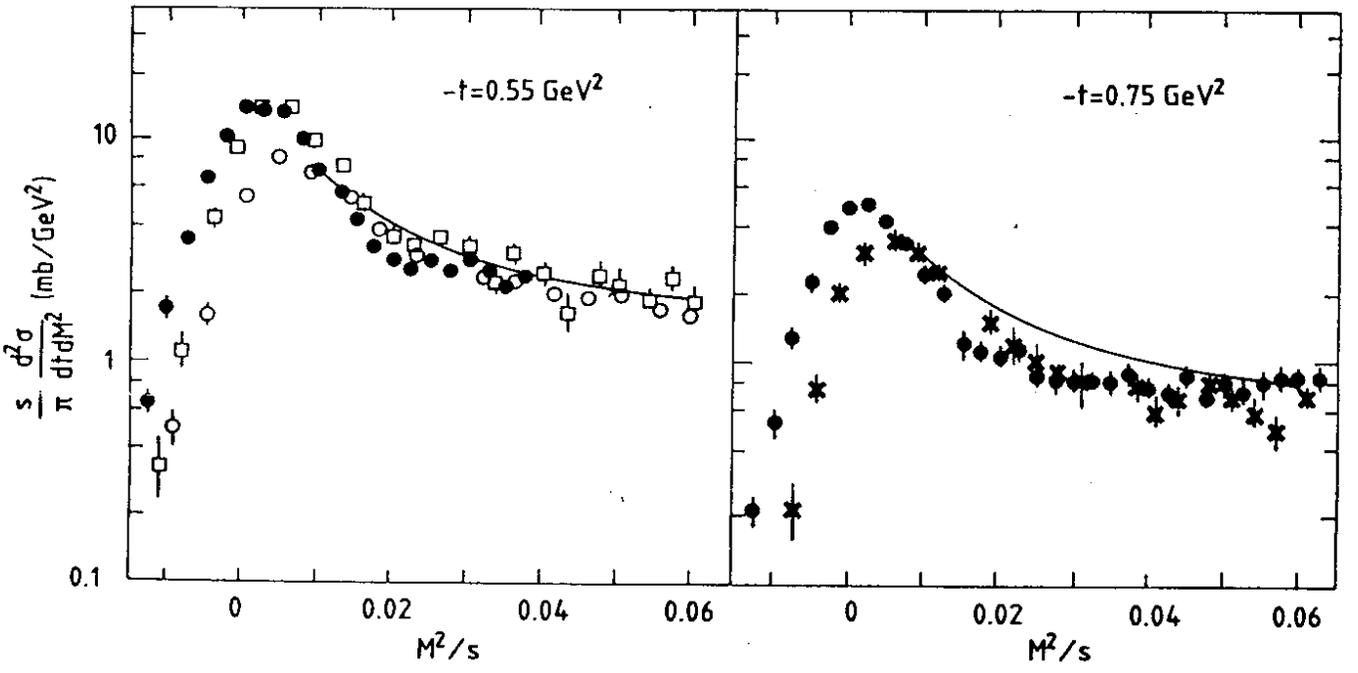

4.9 Calculations of (4.11) by Donnachie and Landshoff (1984). The data points are from the ISR (CHLM Collaboration) and the SPS Collider (UA4).

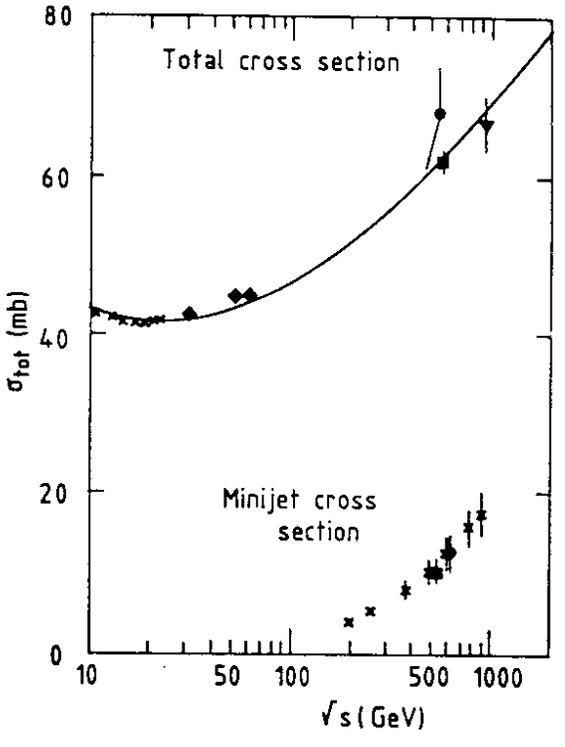

4.10 Measurements by the UA1 experiment of the cross-section for events having minijets with $p_T > 5$ GeV/c , together with data for the total cross-section.

interface between soft and hard collisions.

A minijet is a jet whose transverse momentum p_T is large compared with the nucleon mass, but very much less than the centre-of-mass energy $\sqrt{s}$. Thus the concept is meaningful only for very large $\sqrt{s}$.

When $p_T/\sqrt{s}$ is very small, a calculation using the hard-scattering mechanism of figure 3.13 predicts rather large cross-sections, because parton densities at small x are large. There is no good theoretical understanding of how small p_T is allowed to be with such calculations still being valid, and when p_T is not very large there are theoretical and experimental difficulties in distinguishing the particles in the jet from the other particles produced in the reaction, but certainly the UA1 collaboration at the CERN SPS Collider (Scott, 1986) do find large cross-sections for a value of p_{Tmin} which seems acceptable on both counts. Figure 4.10 shows their measurements of the contribution to the total cross-section of events having one or more pairs of minijets with $p_T > p_{Tmin} = 5\,GeV/c$ and $|\eta| > 1.5$. As can be seen, minijet events form a substantial and increasing fraction of the total cross-section as $\sqrt{s}$ increases. This had indeed been predicted (Horgan and Jacob, 1981), in connection with the correlated rise of mean transverse momenta and rapidity densities, first observed in cosmic Rays.

Up to energies $\sqrt{s}$ of about 50 GeV, the average transverse momentum of particles produced in a reaction is indeed rather constant: see figure 4.11. It is also independent of the other reaction parameters, such as the multiplicity of particles. However, at higher energies it rises with energy $\sqrt{s}$ and also at fixed energy with the multiplicity of particles produced in the

central rapidity region. It seems rather clear that this rise is associated with minijet production.

We have previously said that the total cross-section at high energy can be calculated from pomeron exchange. The conclusion, therefore, is that as $\sqrt{s}$ increases pomeron exchange generates an increasing number of events containing jets of rather high p_T. So as the energy increases "soft" physics merges with "hard" physics,

This hard pomeron coupling is probably related to the quark properties of the pomeron which we wanted to underline in this article despite the fact that the subject is not yet well explored.

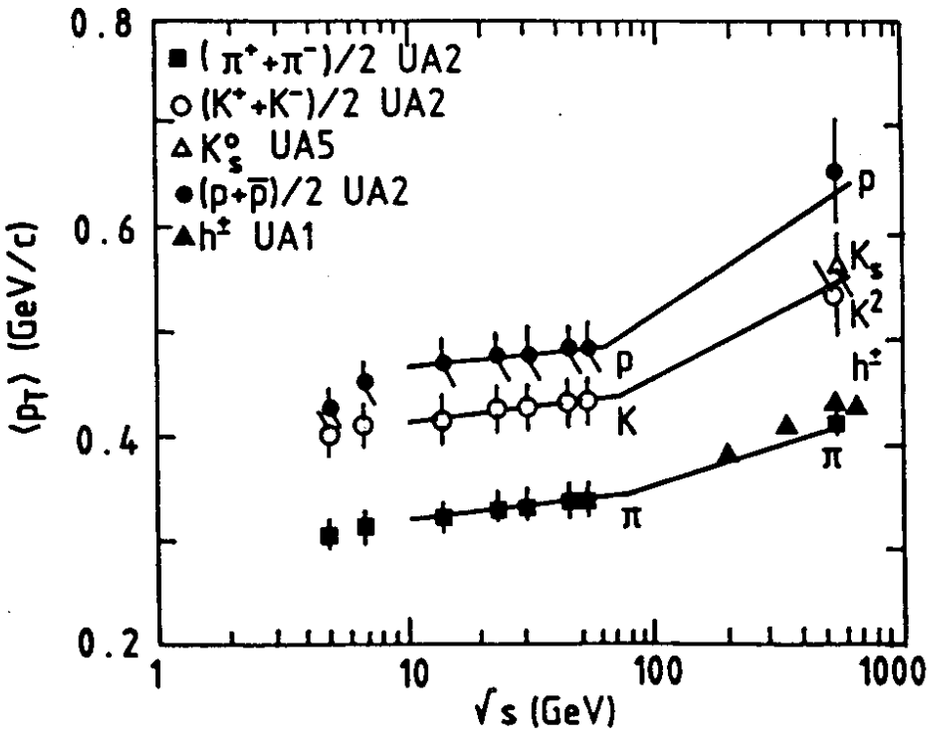

4.11 Average transverse momentum of particles produced in hadron-hadron collisions (from Rushbrooke, 1985).

5. QUARK PLASMA

Deconfinement Phase Transition

It is expected that when matter is raised to sufficiently high temperature T, or when it has sufficiently high baryon number density (or both), a phase transition takes place. Beyond the phase transition, the quarks in the matter can move more or less freely through it over long distances, and are no longer confined within individual hadrons.

In §1 we already discussed why at high temperature we expect the colour field to be no longer confined. We can consider the case of high T from a different point of view. There are frequent energetic collisions between particles, producing pions. At high enough T, or energy density, there are so many pions formed that they effectively coalesce. If one thinks of a pion as a "bag" within which the valence quark and antiquark are confined, at high T the pion bags are squeezed together and the quarks can hop across from one bag to another.

Consider instead high baryon number density, so that there are a lot of quarks very close together. A given quark will not feel any forces from the other quarks far away from it; these forces are screened by the nearer quarks. But the nearby quarks are very close and so the force that they produce is weak, because of asymptotic freedom. So the quarks are subjected to only a weak force, and again they can move rather freely.

In either case, we say that a quark plasma, or more properly a quark-gluon plasma, has been formed. The above arguments are of course not a proof that this will happen, but if a model predicts that it will then they enable us to understand why.

The simplest model is inspired by the bag model of hadrons. In the bag model, a hadron is pictured as a set of quarks moving freely inside a bag. The bag modifies the vacuum inside itself, causing additional energy density B (the so-called "bag constant").

In order to understand how a plasma may occur, we need to remind ourselves about statistical mechanics. We must use the grand-ensemble formalism, since in a relativistic theory the number of particles is not fixed. For example, in thermal equilibrium at high T, there is continual production and annihilation of pions. In the grand-ensemble formalism, we consider an ensemble of systems for which the baryon number and also the energy can vary from system to system, but their totals for the whole ensemble are fixed. That is, only the <u>average</u> baryon number $(N_B - N_{\overline{B}})$ and energy E for each system are fixed. One maximises what turns out to be the entropy S, subject to these two constraints, that is one maximises

$$S + \alpha E + \beta (N_B - N_{\overline{B}})$$

where α, β are Lagrange multipliers. If we introduce $T = -\frac{1}{\alpha}$ and $\mu = \beta T$, and multiply by -T, this is equivalent to minimising

$$\Omega = E - TS + \mu (N_B - N_{\overline{B}}) \qquad (5.1)$$

The quantity Ω is called the thermodynamic potential. It is well known in statistical mechanics that if the surface energy is negligible compared with the volume energy, then

$$\Omega = -PV \qquad (5.2)$$

So if we can calculate Ω we have the equation of state of the system. This calculation is comparatively easy because Ω turns out to be simply related to the partition function Z for the grand ensemble:

$$\Omega = T \log Z \tag{5.3}$$

(in units where Boltzmann's constant is set equal to 1).

In our model, the plasma consists of quarks and gluons that are non-interacting. For non-interacting quarks, the statistical mechanics calculates that the average number of quarks in the energy level ϵ is

$$\frac{\rho(\epsilon)}{e^{(\epsilon - \mu)/T} + 1} \tag{5.4}$$

where $\rho(\epsilon)$ is the degeneracy of the level. Because each quark has 2 spin states and 3 colour states, $\rho(\epsilon) = 6N_f$, where N_f is the number of flavours. The average number of antiquarks in the level is given by a similar formula, with μ replaced by $-\mu$. Hence if $\mu > 0$ there are more quarks than anti-quarks, that is the baryon-number density is positive. If $\mu < 0$ it is negative. The quantity μ is called the chemical potential.

We do not have any constraint on the number density of gluons, so for them there is no chemical potential. For gluons we have instead of (5.4)

$$\frac{\rho(\epsilon)}{e^{\epsilon/T} - 1} \tag{5.5}$$

where, of course, the different sign in the denominator appears

because they are bosons. Now there are again two spin states (the gluons are massless and on-shell, because they are non-interacting), but 8 colour states. So $\rho(\epsilon) = 16$.

From (5.4) and (5.5) one can calculate the average energy density in the plasma. If μ and the quark mass are both 0 the result is

$$\frac{E}{V} = C_{pl} T^4$$

$$C_{pl} = \frac{\pi^2}{90} \left[\frac{7}{8} \cdot 6 N_f + 16\right] \qquad (5.6)$$

One also finds

$$P = -\frac{\Omega}{V} = \frac{E}{3V} \qquad (5.7)$$

Notice that C_{pl} is big, because the square bracket contains contributions from many flavours and colours.

As a very simple model of the hadron phase, pretend that it consists solely of massless pions. Then

$$\frac{E}{V} = C_h T^4$$

$$C_h = \frac{\pi^2}{90} [3] \qquad (5.8)$$

with relation (5.7) again true. This model is very crude, but what matters is that $C_h \ll C_{pl}$.

We still have to incorporate the bag constant B for the plasma phase. We must do this in a way that has proper regard for special relativity, though otherwise there is some freedom in

how we do it. (Remember that we are only making a model, not a proper theory). Let the velocity of the centre of mass of the fluid be $\underline{v}$, and as usual define the 4-velocity $u = (\gamma , \gamma \underline{v})$. When the fluid is at rest on average, $u = (1,0,0,0)$. Consider the tensor

$$T^{\mu\nu} = \left[P + \frac{E}{V}\right] u^{\mu}u^{\nu} - P g^{\mu\nu} \tag{5.9}$$

(which is known as the energy-momentum tensor). It has the property that for the hadron phase, and in the "rest" frame of the fluid of hadrons,

$$T^{00} = \frac{E}{V} = C_h T^4$$

$$T^{11} = T^{22} = T^{33} = P = \frac{E}{3V} \tag{5.10}$$

For the plasma phase, we want a formula similar to (5.9), except that we must introduce the bag constant B. As B is supposed to be a property of the vacuum rather than of the fluid, we must modify the second term rather than the first:

$$T^{\mu\nu} = \frac{4}{3}C_{pl} T^4 u^{\mu}u^{\nu} - \frac{1}{3}C_{pl} T^4 g^{\mu\nu} + B g^{\mu\nu} \tag{5.11}$$

Thus now (compare (5.10))

$$\frac{E}{V} = T^{00} = C_{pl} T^4 + B$$

$$p = T^{11} = \frac{1}{3}C_{pl} T^4 - B \tag{5.12}$$

The formulae (5.10) and (5.12), which give the pressure and energy density in the two phases, are plotted in figure 5.1.

Recall that in thermodynamic equilibrium the thermodynamic potential Ω is minimised. According to (5.2), this means that for a system of given volume V the pressure is maximised. That is, below the "critical temperature" T_c at which the two pressure curves cross, the equilibrium configuration is the hadron phase, while above T_c it is the plasma phase.

If the system is heated slowly up to the critical temperature, it will remain at this temperature until a further quantity of heat 4B per unit volume has been added. This is the latent heat needed to cross from one curve to the other in the energy-density plot. When as in this simple model, the energy-density curve has a discontinuity at $T = T_c$, the phase transition is called "first-order". It is an important question whether for real matter the phase transition is in fact first-order; it could be second-order, in which case the energy density is continuous but its slope (the specific heat) is discontinuous. It could be more complicated with percolation between the two phases.....

Unless the transition between the two phases occurs very slowly, it is a very complicated non-equilibrium process. In order to understand the significance of the transition being first-order, imagine that the system is in the plasma phase and is cooled rapidly down to below the critical temperature. If it were to remain in equilibrium, it would change to the hadron phase. However, in §4 we saw that it needs time for quarks to hadronise (the "formation time" of about 1 fm in the quark rest frame). So rather than passing to the hadron phase immediately, the system will continue for a while in the plasma phase: it becomes supercooled. Likewise, when the system is heated rapidly from the hadron phase it can become superheated. As we shall see, this could be important for detecting that a quark plasma

has been created in an experiment.

Lattice gauge theory

In order to calculate the equation of state properly, we must use the quark and gluon interactions of the QCD Lagrangian. There is then no need to put in a bag constant B by hand as we did in our two-phase approach. For temperatures near $T = T_c$ and below one cannot use perturbation theory, and the only calculational method we have is lattice gauge theory.

In lattice gauge theory, space-time is made discrete, so that it becomes a lattice of points. One calculates with a finite spacing a between the points, and then hopes to recover the continuum theory by extrapolating the results of the calculations so that $a \to 0$. Since space-time has infinite volume one obviously ought to take a very large number of points in the lattice, but this needs huge computing power, so that in practice at most a few thousand points are used.

A good introduction to lattice gauge theory is the book by Creutz (1983), while for the physics of the quark plasma there is the book by Müller (1985). Most calculations include only gluons; quarks are much harder to deal with particularly if they have light masses.

For $T \gg T_c$, the force between the gluons is weak, for the reasons given at the beginning of this section. So $E/V = C_{pl} T^4$, with $C_{pl} = 16\pi^2/90$, is a good approximation: see (5.7). One can correct for the presence of the weak force using perturbation theory on the lattice. Taking the lattice spacing $a \neq 0$ removes the divergences from the perturbation theory, so this is yet another renormalisation scheme, with its own value of Λ. If

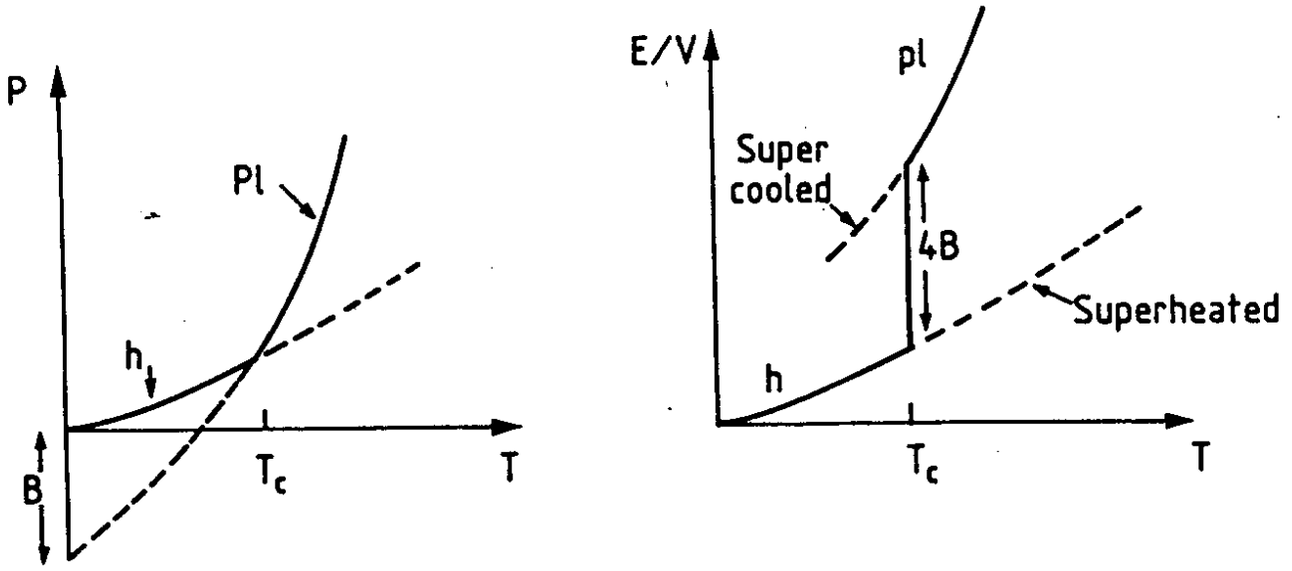

5.1 Plots of the pressure and energy density in the hadron and plasma phases, according to the simple model. The solid curves correspond to thermodynamic equilibrium.

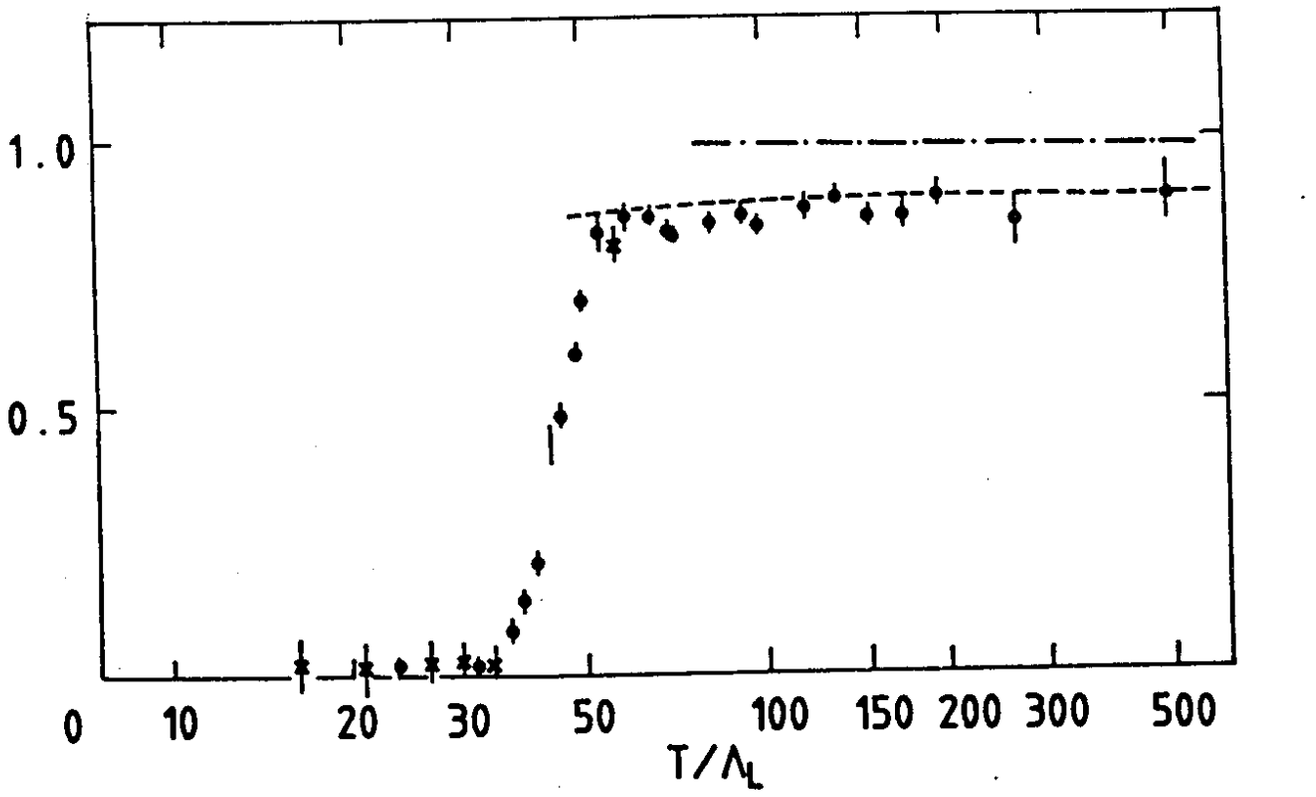

5.2 Energy density for a plasma of gluons, divided by $C_{pl} T^4$. The dashed line is a perturbation-theory calculation. (From Heller and Karsch, 1985.)

$\Lambda_{\overline{MS}} \approx 150$ MeV, the lattice Λ is a few MeV. Figure 5.2 show the result of a lattice calculation of E/V divided by $C_{pl} T^4$; this is compared in the figure with the perturbation-theory calculation.

The results of the lattice calculation have error bars because the Monte-Carlo calculational technique induces errors. It would appear that there is something close to a first-order phase transition, with a critical temperature of about 200 MeV. Because of the finite size of the lattice, one cannot strictly have a phase transition at all. Whether there really is a first-order phase transition in the infinite-volume continuum limit, particularly when quarks are included, is still open to debate. Notice also that so far there are very few calculations for non-zero baryon-number density ($\mu \neq 0$). While we do not know the exact nature of the transition it has to take place with a large amount of heat released or absorbed ((5.6) and (5.8)) through the transition.

Collisions of Heavy Nuclei

When a spherical nucleus has large momentum, it becomes pancake-shaped because of Lorentz contraction. If two high-momentum nuclei collide head-on, such that the collision more or less stops them, a lot of energy is dumped into the small pancake-shaped volume in which they coalesce. Maybe the energy density is high enough to create a quark plasma. Experiments to investigate this are in progress at CERN, though as they are fixed-target experiments it may be that not enough energy will be dumped. There are tentative plans to study Au-Au collisions in a collider constructed in the ISABEL tunnel at Brookhaven, with a centre-of-mass energy of 200 GeV/nucleon. The energy dumped should surely then be sufficient.

There are a number of obvious questions:

1. 1. *How much energy is dumped into unit volume?*

The simplest calculations use the concept of "nuclear stopping power". It is noted that in pp collisions the leading outgoing nucleon on average loses 60% of its energy, and more in proton-nucleus collisions. It is assumed that this lost energy is dumped into a "fireball", and that if the energy density in this fireball is high enough a plasma is formed. This will surely not be the case in pp collisions, but it should happen in nucleus-nucleus collisions. Other calculations are more sophisticated, for example they attempt carefully to keep track of the separate collisions of the nucleons within the nuclei. Estimates of the energy dumped into unit volume vary widely, but they agree that of the order of 1 GeV/fm^3 can be achieved fairly easily.

2. *What energy density is needed for a phase transition?*

The crudest way to estimate the order of magnitude required is to say that the quarks in the nucleon bag move more or less freely. The energy density within the bag is (1 GeV)/($\frac{4}{3}\pi$ fm^3) $\approx \frac{1}{4}$GeV/fm^3 . So the critical energy density should be not too far from this value. The lattice gauge theory calculations support this.

3. *Does the plasma have time to reach thermal equilibrium?*

When the plasma is created, it is certainly not in thermal equilibrium. Many quark and gluon collisions are surely needed to achieve equilibrium. The calculation of the rate at which they occur is a complicated non-equilibrium transport problem and is very uncertain. It is believed, however, that there is ample time for equilibrium to be reached before the plasma hadronises.

4. *How does the plasma expand and change into ordinary matter?*

Calculations of this are very model dependent. Typically, they use the relativistic form of the Navier-Stokes equation of fluid dynamics to treat the plasma as if it were a continuous fluid. It is found that as the plasma expands longitudinally, a rarefaction shock wave propagates transversely inwards. The plasma cools as it expands. As we have discussed, if the phase transition is first order (or nearly so), when T falls below T_c the plasma at first becomes supercooled. As hadronisation begins to occur, bubbles of supercooled plasma remain embedded in the ordinary matter. What happens to these is investigated using a relativistic version of combustion theory. One possibility is that they explode and spray hadrons in all directions.

5. *What experimental signals will indicate that a phase transition has occurred?*

A number of possible answers to this question have been suggested. For example, an exploding bubble would produce large transverse energy, uniformly distributed in azimuthal angle and confined to a small interval of rapidity. Also, the plasma should have a substantial strange-quark content, so that rather more strange hadrons should be produced than in normal events. The temperature of the plasma will not be high enough for it to contain a significant number of charmed quarks, though some will be produced as a result of collisions between the quarks and/or gluons in the plasma. Photons and leptons will be produced in the same way. The production may be calculated using perturbation theory; examples of the relevant diagrams are drawn in figure 5.3. The cross-sections calculated from these diagrams must be convoluted with the statistical-mechanical momentum distribution of the initial quarks and gluons, corresponding to the

temperature of the plasma.

It has come to be realised that there is not likely to be any one signal that will give a clean sign that a plasma has been produced. In each case, the problem is to distinguish the signal for new physics from the tail of the corresponding distribution produced by old physics. What must be done, therefore, is to look for events where there are several apparent signs that something new has occurred - one is unlikely simultaneously to hit the tails of several old-physics distributions. Of course this makes the experiments very hard. The theory is also not well understood, but it is very interesting because it brings together so many different branches of physics - particle physics, statistical mechanics, fluid mechanics, combustion theory etc. So altogether the subject is very difficult, but with any luck it will bring the next big new discovery at CERN.

The present CERN program is based on an Oxygen beam of 225 GeV/c per nucleon with experimentation starting in late 1986. In late 1987 one hopes to have a sulphur beam at the same energy per nucleon and intensity. Since to a large extent a proton is a broad-band beam of quarks and gluons, so is a nucleus. The only difference is that the density is higher! With such energies one has good reason to hope that, in head-on collisions on a heavy nucleus target, the energy density reached will be such that a quark plasma can be formed. This will be done in an explosive mode since, once formed, it will cool down and hadronize very fast, with a time scale of 10^{-23} sec. One may say that the corresponding Hubble Constant is 10^{17} times that of our Universe when it went through that transition, a few microseconds after the Big Bang.

Nevertheless, if we cannot see the Cat we can hope to see its Grin in the form of specific effects associated with the transient existence of a quark plasma phase i.e. peculiar photon or lepton pair yield, peculiar, strange or charmed particle yields, peculiar pion density, the key point being to find correlations between such possible peculiar distributions. The five experiments which will take data during the forthcoming run will indeed all look at different effects at the same time in the hope of seeing correlations among peculiar distributions. It is our first look at high quark and energy density over a sizeable volume and we may have a few surprises. Actually the most exciting thing would be to find new long-lived states built out of larger numbers of quark. Nothing prevents their existence in present theories and they could be formed in the very high quark density system which will be studied.

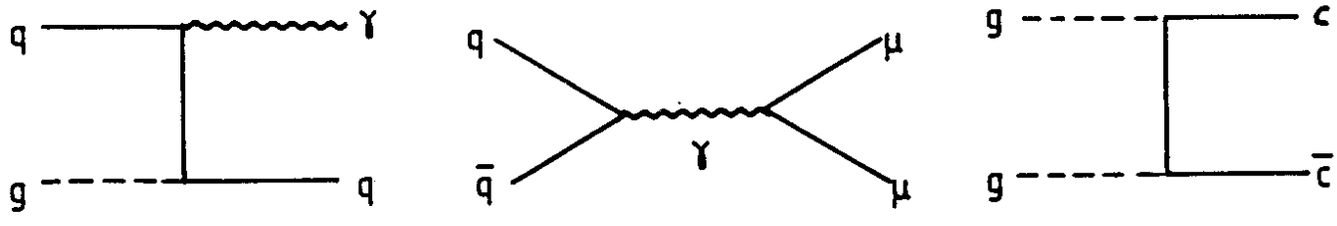

5.3 Production of photons, muons and charmed quarks by collision between quarks and/or gluons in the plasma.

6. EXPLORING DOWN TO 10^{-19}m

In 1907, J.J. Thomson wrote,"There is indeed one part of Physical Science where the problems are very analogous to those dealt with by the metaphysicians... To some men this side of physics is particularly attractive. They find in the physical Universe with its myriad phenomena and apparent complexity a problem of inexhaustible and irresistible fascination. Their minds chafe under the diversity and complexity they see around them, and they are driven to seek a point of view from which phenomena as diverse as those of light, heat, electricity and chemical action appear as different manifestations of a few general principles". It is clear that this approach has paid handsome dividends since and that we have now actually reached even beyond that point of view, a unique gauge principle being at the origin of all the interactions as described in the framework of the Standard Model, which is QCD together with the Glashow-Salam-Weinberg electroweak theory. We described in sections 2 and 3 how the Standard Model gives a good description of the structure of matter at the scale of 10^{-18}m , corresponding to probing with momentum in the 100 GeV range.

Novelty around the corner

The very successes of our present theoretical picture throw up some challenging questions. The first concerns the number of parameters in the Standard Model, at least 17, whose values have to be fixed from experiment. These include 3 gauge couplings and the masses of all the quarks and charged leptons, together with angles that specify the mixings of the quarks under the weak couplings. An obvious problem is how can one reduce this number.

The Glashow-Salam-Weinberg model unifies in some sense the electric and weak interaction, making them equal in strength at the scale of 10^{-18}m or 100 GeV. At the same time it reduces the number of parameters that electroweak theory might have needed; for example it relates the ratio of the electric and weak couplings to the ratio of the W and Z masses (see, for example, the book by Aitchison, 1982 or by O'Raifeartaigh, 1986). An obvious thing to try is to reduce the number of parameters further by constructing a grand unified theory (GUT), in which QCD is also included in the unification. The three coupling constants of the standard model all run with the renormalisation scale μ in a way similar to $\alpha_s(\mu^2)$ in (3.11). (The constant $1/\beta_0$ is different for each; it changes according to the gauge group.) At values of μ of the order of 10^{15} GeV they become nearly equal, which supports the belief that grand unification does occur. This means that on the scale of 10^{15} GeV the theory has a larger symmetry, which at lower energies is broken down to the $SU(3) \times SU(2) \times U(1)$ symmetry of the standard model. The most economical candidate for this larger symmetry group is SU(5); this and other groups have been studied extensively (see O'Raifeartaigh, 1986). GUTs have many encouraging features, though the failure to detect proton decay, with a predicted lifetime of the order of 10^{32} years or less, is something of a setback.

It might seem that 10^{15} GeV is in any case too high an energy scale to have any simple relevance to physics at the present 100 GeV level. However, this is untrue.

The Standard Model includes scalar fields, the Higgs fields, which are at the core of the symmetry breaking. The masses of these are not determined in the model, but it would be embarrassing if they were too much above the Z mass. This is because in

WW scattering there must be a cancellation between photon, Z and H exchanges, so as to avoid the breakdown of unitarity in the perturbative approach (Lee, Quigg and Thacker, 1977), and this can work properly only if the Higgs mass is not too large, say 1 TeV at most. But in a simple GUT the square of the mass of a scalar field is liable to suffer a radiative correction of order $g^2M_X^2$, where g is the gauge coupling and M_X is the unification mass scale. (For a fermion it is only of order $g^2m^2\log^2(M_X/m)$, where m is the fermion mass, and so there is no obvious problem.) Of course one could choose the bare mass of the field so as to cancel this, but this would need a fine tuning to about one part in 10^{13}, so that we cannot seriously consider it with anything but awe. Because of this "hierarchy problem" (too strong a hierarchy between very different scales), one must be uneasy about GUTs that have no new physics between 100 GeV and 10^{15} GeV.

One way out is to introduce supersymmetry (see, for example, the book by Freund, 1986). Then each fermion in the theory has a boson partner with a related coupling, and there are systematic cancellations between fermion-loop and boson-loop contributions to the radiative corrections. Of course supersymmetry is a broken symmetry: for example, the mass of the selectron, the as-yet-undiscovered scalar partner of the electron, is certainly much greater than that of the electron. This means that the cancellations are not exact; rather, the correction to the Higgs squared mass would be of order $g^2\Delta m^2$, where Δm is the typical mass difference between supersymmetric partners. So if the Higgs mass is not to exceed a TeV or so, the same must be true of the masses of the supersymmetric partners of the known particles.

An alternative possibility is that Higgs particles are composite systems (see, for example, Kaul, 1983 or Schrempp, 1986).

Then the relevant energy scale for radiative corrections to their mass is that at which they break up into their constituents. A particular example is the "extended technicolour" model, where the Higgs mesons are bound states of new kinds of particles, technifermions and their antiparticles. For the reasons we have already discussed, their masses should be at or below the TeV level. Such models do have some problems with unwanted couplings and particles, yet the idea of composite Higgs particles does have some appeal.

The key point is that there must be new physics at the TeV scale, even if we do not know precisely what form it will take. This new physics is of extreme interest because

(i) It should tell us the way Nature operates to break symmetries which are fundamental to the consistent structure of gauge theories and by the same token should shed light on a possible dynamical origin of masses

(ii) It should tell us how our present and obvious successes are compatible with a grand unification which appears as a great theoretical challenge.

Looking around the corner

There is good reason, then, to contemplate an e^+e^- collider with a centre-of-mass energy of a few TeV (it would have to be a linear collider, at such an energy). Alternatively, one would need a hadron-hadron collider with an order of magnitude greater energy, so that the quark-quark or gluon-gluon collisions are again at a few TeV. Again the goal is to explore the dynamics of the symmetry breaking of electroweak theory, and the origin of masses.

New particles in the TeV range will decay into jets that have very high transverse momenta. A key element in the enthusiasm for experimenting with hadron colliders in this new energy domain is the clarity of the event structure at the CERN $p\bar{p}$ collider (figure 1.1), which strongly encourages the hope that jets associated with new massive particles will be seen very clearly. Studies for new colliders have been undertaken both in the United States and in Europe. In the U.S. it is hoped to build a 40 TeV proton-proton collider, the Superconducting Super Collider (SSC), while the LEP tunnel at CERN could accommodate a 17 TeV Large Hadron Collider (LHC). For details of the studies, see the ECFA-CERN Workshop proceedings (1984) and the extensive Snowmass SSC studies (1985).

The incident hadrons can be regarded as broad-band beams of quarks and gluons. To estimate reaction rates, consider the Drell-Yan process of section 2 as a prototype. If we integrate (2.27) over x_F , we may write the result in the form

$$\frac{d\sigma}{dm^2_{\mu\mu}} = \frac{8\pi\alpha^2}{9m^4_{\mu\mu}} \sum_i e_i^2 \tau \frac{dL_i}{d\tau} \qquad (6.1)$$

Here the sum runs over quark flavours i and e_i is the fractional charge of the quark. The quantity $dL_i/d\tau$, which from (2.28) has the form

$$\frac{dL_i}{d\tau} = \int_\tau^1 \frac{dx}{x} \left[q_i(x)\bar{q}_i\left(\frac{\tau}{x}\right) + \bar{q}_i(x) q_i\left(\frac{\tau}{x}\right) \right] \qquad (6.2)$$

is called the differential luminosity. It measures the relevant overlap of parton densities, and clearly it falls off with increasing τ , as one runs out of partons sufficiently energetic

to produce the mass $m_{\mu\mu}$. Similarly, the cross-section for the production of a particle of mass M by the fusion of two partons i and j (either quarks or gluons) with coupling g_{ij} may be written as

$$\sigma = \frac{\pi}{M^2} g_{ij}^2 \tau \frac{dL_{ij}}{d\tau} \qquad (6.3)$$

where $\tau = M^2/s$.

The relation (6.3) illustrates some important points. The energy scale under study sets the value for M. If we are interested in 1 TeV, and use a collider 10 times the energy of the present SPS collider so that τ takes the same value as at present corresponds to W,Z production, the cross-section for the same coupling is well over two orders of magnitude down. Two orders of magnitude come from the M^2 in the denominator, and there is a further reduction because for $\tau = 0.01$ scaling violation reduces the differential luminosity. Figure 6.1 shows the reduced cross-section $\sigma/g_{ij}^2\pi$ for the case where the particle is produced from gluon-gluon fusion, plotted as a function of M for various machine energies $\sqrt{s}$. Notice the sharp fall-off with increasing M even when $\sqrt{s}$ is large. For example, suppose that one needs the reduced cross-section to be at least 1 in order to achieve an acceptable production rate. Then it takes a hundredfold increase in $\sqrt{s}$ to compensate for a tenfold increase of M. In practice, one runs out of rate before one runs out of energy.

The production rate is the cross-section times the machine luminosity. Nevertheless the luminosity that can reasonably be expected from a pp collider with an energy of order 20 TeV is about $10^{33}\,cm^{-2}\,s^{-1}$. This is some 4 orders of magnitude greater

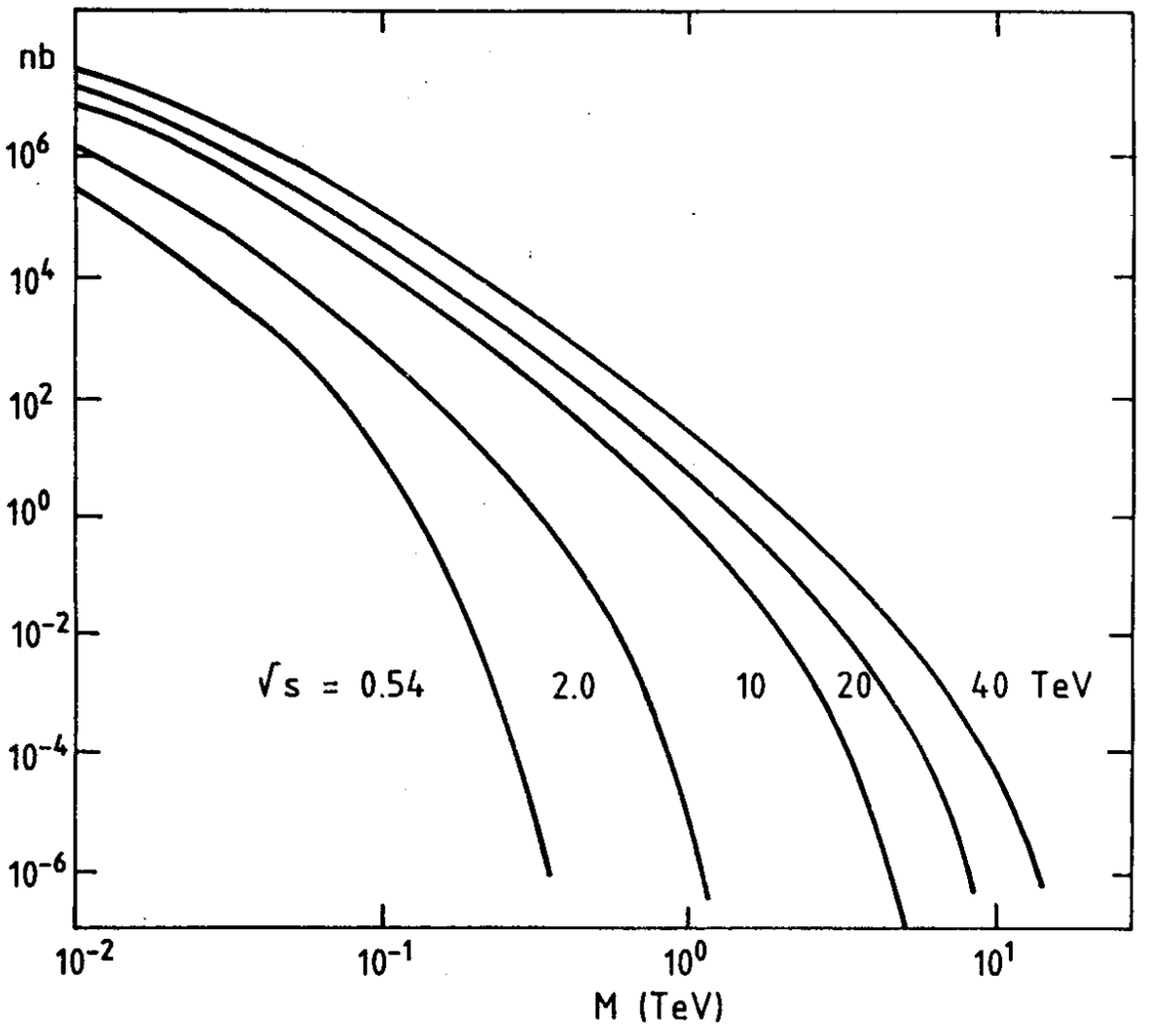

6.1 The reduced cross-section $\sigma/g_{ij}^2\pi$ for the case of gluon-gluon fusion.

than that of the SPS $p\bar{p}$ Collider, which is severely limited by the intensity of the antiproton source. So at $\sqrt{s}$ = 20 TeV, structures in the TeV range will be produced at rates some thousand times that of W production at the SPS Collider. One can be confident about rates.

But a high production rate is not sufficient: one must be able to separate the signal from the background. The beautiful jet signal of today (figure 1.1) will be the background of tomorrow, and a serious one. Suppose, for example we take $\sqrt{s}$ = 20 TeV and M = 2 TeV. Consider the case where the particle M is produced at rest and decays into two jets emerging at 90° to the colliding beams, that is two jets each with transverse momentum p_T = 1 TeV. Even if the coupling g_{ij} is as large as 1, which is unlikely, the rate obtained from figure 6.1 is only about the same magnitude as the background calculated from figure 3.13. In order to overcome this difficulty, it will often be necessary to look for specific decay modes, just as in the search for the W at the SPS Collider one had to look for the leptonic decay mode: the jet decay has a larger yield, but is submerged in background.

Such problems have been extensively investigated in the studies in the United States and at CERN. The conclusion is that if nature chooses supersymmetry or technicolour the consequences should be clearly visible, with large enough cross-sections and signals. The Higgs particles may be difficult to detect, but supersymmetric or technicolour particles, and more conventional heavy fermions or new vector bosons, will be found if their masses are less than a TeV or so.

Even if there are not surprises to be discovered, there must be some new things, which presently appear of primordial

interest.

The theory of everything

We have described how attempts to unify the strong and electroweak forces in a GUT at the scale of 10^{15} GeV reflect back on physics at 100 GeV. Very promising attempts are now being made to include also gravity in the formalism, so as to obtain a theory of everything. The unification scale is now the Planck mass, 10^{19} GeV. The corresponding length scale is 10^{-35}m . In the theory it is imagined that, if it were possible to probe them on this scale, quarks and leptons would appear as excitations of one-dimensional extended objects rather than as points. The theory incorporates supersymmetry; and is known as superstring theory (Green, Schwarz and Witten, 1986). For the first time, it seems to offer the possibility of a consistent quantum theory of gravity.

The theory is very promising but can be formulated only in a space-time having 10 dimensions. Six of these dimensions have to "compactify": they curl up on themselves at a distance of 10^{-35}m , leaving the 4 dimensions of present-day physics. Consistency requires symmetry associated with well-defined groups.

At present it is too early to draw any definite conclusions about the phenomenological consequences at accessible energies. Yet the known particles should be in representations of rather high dimensions with many new partners whose mass should not be too much greater than that of the W and Z (Ellis, 1986). A theoretical path often followed starts from a $E(8) \times E(8)$ symmetry, particles being associated to representations of an $E(6)$ subgroup of one of the $E(8)$ broken to $SU(3) \times E(6)$ through compactification.

Our known particles should have many partners beside their super-symmetric ones! Physics at one TeV at the parton level should then be a cornucopia of particles and the source of much new knowledge.

Whether one looks from below, from present energy to the grand unification scale and beyond, or, from above, starting with a quantum theory of gravity at the Planck mass, there should, then, be a great deal of new activity "around the corner". Over the past decade or so many basic questions have been answered. We now have

The nature of the weak force

The nature of the strong force

The structure of hadrons.

We now have to look at deeper questions, such as

What is the origin of the mechanism for symmetry breaking and mass?

What kind of unification is there beyond the Standard Model?

Are all interactions but different facets of a quantum theory of gravity?

REFERENCES

Aitchison I.J.R. 1982 "An informal Introduction to Gauge Theories", Cambridge University Press.

Altarelli G. 1982 Phys. Rep. 81, 1.

Altarelli G., Ellis R.K. and Martinelli G., 1978 Nuclear Physics B143, 521.

Aubert J.J. et al. 1982 Physics Letters 114B, 291.

Bjorken J.D. 1969 Phys. Rev. 179, 1547.

Busza M. 1976 Proc. VII International Colloquium on Multiparticle Reactions, Tutzing

Close F.E. 1979 Rep. Prog. Phys.

Collins J.C. 1984 "Renormalization", Cambridge University Press.

Collins P.D.B. 1977 "An Introduction to Regge Theory", Cambridge University Press

Collins P.D.B. and Gault F. 1982 Physics Letters 112B, 255.

Creutz M. 1983 "Quarks, Gluons and Lattices", Cambridge University Press.

De Tar C.E., Ellis S.D. and Landshoff P.V. 1975 Nuclear Physics B87, 176.

Donnachie A. and Landshoff P.V. 1979 Z. Phys. C2, 55

1984 Nuclear Physics B244, 322

1986 Nuclear Physics B267, 690.

ECFA-CERN Workshop Proceedings 1984, CERN Report 84-10.

Eisele F. 1986 Rep. Prog. Phys.

Ellis J.R. 1986, CERN preprint TH 4474.

Ellis S.D., Kleiss R. and Stirling W.J. 1986 Physics Letters 167B, 464.

Faessler M.A. 1984 Proc. Cargese Summer School on Heavy Ion Collisions.

Feynman R.P. and Field R.D. 1978 Nuclear Physics B136, 1.

Freund P.G.O. 1986 "Introduction to Supersymmetry", Cambridge University Press.

Green M.B., Schwarz J. and Witten E. 1986 "Superstrings", Cambridge University Press.

Heller V. and Kersch F. 1985 Nuclear Physics B251, 254.

Hendry A.W. and Lichtenberg D.B. 1978 Rep. Prog. Phys.

Horgan R.R. and Jacob M. 1981 CERN Report 81-04.

Jaroskiewicz G.A. and Landshoff P.V. 1974 Phys. Rev. D10, 170.

Kaul R. 1983 Rev. Mod. Phys. 55, 449.

Kenyon I.R. 1982 Rep. Prog. Phys.

Landshoff P.V., and Polkinghorne J.C. 1971 Nuclear Physics B32, 541.

Landshoff P.V. and Stirling W.J. 1982 Z. Phys. C14, 251.

Lee B.W., Quigg C. and Thacker H.B. 1977 Phys. Rev. Lett. 38, 883.

Muller B. 1985 "The Physics of the Quark-Gluon Plasma", Springer-Verlag.

Niedermayer F. 1974 Nuclear Physics B79, 355.

O'Raifeartaigh L. 1986 "Group Structure of Gauge Theories", Cambridge University

Press.

Pauss F. et al. 1985 Z. Phys. C27, 211.

Review of Particle Properties 1986 Physics Letters 170B, 1.

Rushbrooke J.G. 1985 Proc. European Physical Society Meeting on High Energy Physics, Bari.

Saxon D.H. 1985 Proc. European Physical Society Meeting on High Energy Physics, Bari.

Schrempp B. 1986 Proc. VI International Conf. on Proton-Antiproton Physics, Aachen.

Scott W. 1986 Proc. XXIII Int. Conf. on High Energy Physics, Berkeley.

Smith A.M. et al. 1985 Physics Letters 163B, 267.

Snowmass SSC Studies 19.

Thomson, J.J. 1907.

Watkins P. 1986 "Story of the W and Z", Cambridge University Press.

Wu S.L. 1984 Phys. Rep. 107, 59.